

Solvable entanglement dynamics in quantum circuits with generalized space-time duality

Chuan Liu^{1,*} and Wen Wei Ho^{1,2,†}

¹*Department of Physics, National University of Singapore, Singapore 117551*

²*Centre for Quantum Technologies, National University of Singapore, 3 Science Drive 2, Singapore 117543*

(Dated: March 18, 2025)

We study the non-equilibrium dynamics of kicked Ising models in 1 + 1 dimensions which have interactions alternating between odd and even bonds in time. These models can be understood as quantum circuits tiling space-time with the generalized space-time dual properties of tri-unitarity (three ‘arrows of time’) at the global level, and also second-level dual-unitarity at the local level, which constrains the behavior of pairs of local gates underlying the circuit under a space-time rotation. We identify a broad class of initial product states wherein the effect of the environment on a small subsystem can be exactly represented by influence matrices with simple Markovian structures, resulting in the subsystem’s full dynamics being efficiently computable. We further find additional conditions under which the dynamics of entanglement can be solved for all times, yielding rich phenomenology ranging from linear growth at half the maximal speed allowed by locality, followed by saturation to maximum entropy (i.e., thermalization to infinite temperature); to entanglement growth with saturation to extensive but sub-maximal entropy. Intriguingly, for certain parameter regimes, we find a nonchaotic class of dynamics which is neither integrable nor Clifford, exemplified by nonzero operator entanglement growth but with a spectral form factor which exhibits large, apparently time-quasiperiodic revivals.

Introduction.—Understanding the dynamics of nonequilibrium quantum many-body systems is one of the central challenges in modern physics: it finds relevance in diverse topics ranging from thermalization [1–4] to information scrambling [5–10]. Dynamics in the far-from-equilibrium regime though is typically difficult to describe, due to the large build-up over time of entanglement. Exact classical simulations are limited to small system sizes, while approximate methods like mean-field theory [11] and matrix product states [12–15] can deal with large sizes but quickly lose validity at late times. Solvable models of interacting quantum dynamics are thus highly valuable, but rare. Current well-known examples include integrable systems [16–19], Clifford circuits [20–23], as well as the recently introduced class of dual-unitary quantum circuits in which local gates are unitary in both space and time directions [24–29], a realization of a more general concept of space-time duality [24, 30–35] wherein roles of space and time can be interchanged.

In this Letter, we introduce a family of kicked Ising models in 1D that have interactions alternating between odd and even bonds in time, which we call the “alternating kicked Ising model” (AKIM). These models exemplify a general construction yielding quantum circuits with generalized space-time duality beyond dual-unitarity, via tiling of space-time with local gates which endow the system with multiple ‘arrows of time’, tied to the symmetries of the underlying lattice. For the AKIM, this takes the form of a hexagonal lattice, such that it possess the global property of tri-unitarity (three ‘arrows of time’), but which goes beyond the local tri-unitary framework of Ref. [36]. We also find that the AKIM possesses the

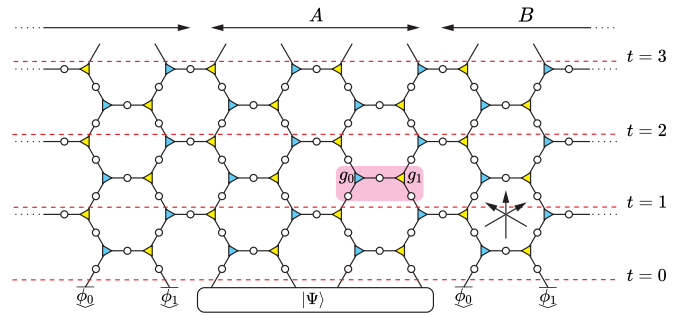


FIG. 1. Quantum circuit representation of the AKIM as an (unnormalized) tensor network tiling space-time in a hexagonal fashion, making evident that there are three ‘arrows of time’: ‘evolution’ of the circuit along any one of the black arrows appears unitary. The circuit can be understood as built up from two-local 2DU gates $u(g_0, g_1)$ (pink shaded box), where the blue (yellow) triangles on the vertices carry phase factor $g_0(g_1)$.

property of ‘second level dual unitarity’ (2DU), a recent hierarchical generalization of dual-unitarity [37]. Thus, our geometric picture offers complementary insights into constructing models with generalized space-time duality like 2DU and possibly beyond (though see related ideas by Ref. [38]).

We show that because of these properties, the AKIM has local entanglement dynamics that can be efficiently classically computed, and under certain conditions even analytically solved, displaying rich phenomenology. Interestingly, we find that dynamics of the AKIM ranges from quantum chaotic, to non-chaotic but which is neither Bethe-integrable nor Clifford. Our results extend our knowledge of solvable interacting quantum dynamics,

yielding yet more analytical testbeds to probe interesting physical phenomena like thermalization and beyond [39–43], quantum chaos [44, 45], and nonequilibrium dynamical phases [46–51].

Model.— Consider discrete-time dynamics on a 1D chain of qubits, with each time step $t \in \mathbb{N}$ governed by the unitary $U = U_e U_o$, where $U_{o/e} = e^{-iH^{(o/e)}} e^{ih \sum_{i=1} \sigma_i^y}$ and

$$H^{(o/e)} = J \sum_{\substack{(i,i+1) \in \\ \text{odd/even bonds}}} Z_i Z_{i+1} + \sum_i (g_i \bmod 2/2 + \pi/4) Z_i. \quad (1)$$

Here X_i, Y_i, Z_i are Pauli matrices on site i . U describes time-evolution alternating between two Ising models which act only on odd or even bonds with strength J , subject to dimerized longitudinal fields g_0, g_1 , and interrupted by global transverse kicks of strength h , hence its name ‘‘AKIM’’. We take $J = h = \pi/4$, and allow g_0, g_1 to be arbitrary. Defined this way, the model is time-periodic i.e. Floquet. Due to reflection symmetry, dynamics at (g_0, g_1) is equivalent to that at (g_1, g_0) , and so we focus on $0 \leq g_0 \leq g_1 \leq 2\pi$.

The physical setting of interest is of local thermalizing dynamics following a quantum quench. Concretely, we focus on a small contiguous subsystem A of even number of qubits N_A deep in the bulk and prepared in pure state $|\Psi\rangle$ (see Fig. 1); and assume the infinitely-large complement B is prepared as a dimerized product state $\prod_i |\phi_0\rangle_{2i-1} |\phi_1\rangle_{2i}$. We track A ’s state over time, given by the reduced density matrix (RDM) $\rho_A(t)$, and desire to understand its entanglement entropy $S(t) = -\text{Tr}(\rho_A(t) \log_2 \rho_A(t))$.

Quantum circuit equivalent \mathcal{E} generalized space-time duality.— Before solving for the AKIM’s entanglement dynamics, we note that the AKIM exemplifies a general construction of quantum circuits with generalized space-time duality. To see this, first observe that U is expressible as a brickwork quantum circuit composed of the two-local gates

$$u(g_0, g_1) = (P(g_0) \otimes P(g_1)) CZ(H \otimes H), \quad (2)$$

where $CZ, H, P(g_i) = \text{diag}(1, e^{ig_i})$ are the standard qubit control-Z, Hadamard, and phase gates respectively. Note when $g_0 = g_1 = 0$, u is equivalent (locally) to the CNOT gate, such that the circuit describes the kinetically-constrained deterministic Floquet quantum East model (DFQE) [52–55], whose entanglement dynamics was recently solved in [53]. Our work advances conceptually that the DFQE lies in a much more general class of entanglement-solvable quantum circuits.

We then introduce a tensor network (TN) representation, using basic tensors

$$\begin{array}{c} z_2 \\ | \\ g \\ | \\ z_1 \end{array} \begin{array}{c} z_3 \\ | \\ z_2 \\ | \\ z_1 \end{array} = \delta_{z_1 z_2 z_3} e^{ig(z_1)}, \quad \begin{array}{c} z_2 \\ | \\ z_1 \end{array} = (-1)^{z_1 z_2} / \sqrt{2}, \quad (3)$$

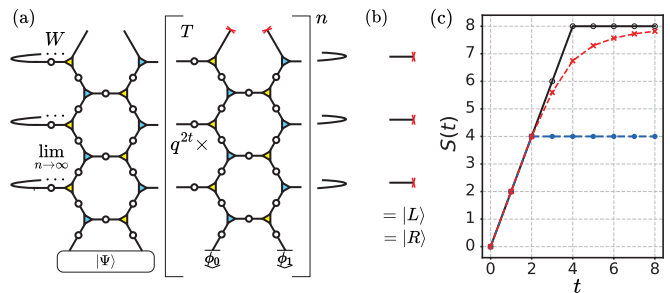


FIG. 2. (a) Computation of RDM $\rho_A(t)$ using spatial transfer matrices T and temporal-to-spatial map W . (b) Left and right eigenvectors of T : a product of t Bell states. (c) Entanglement dynamics of A with $N_A = 8$. Black line: maximum-entanglement-solvable dimerized product states at $g_0 = 0$ (arbitrary g_1), as well as $g_0 = g_1 = \pi/2$, showcasing linear ramp with rate 2 till saturation at maximal entropy. Blue dash: $|z\rangle|z\rangle \cdots$ at $g_0 = g_1 = \pi/2$, showing exact linear ramp till saturation at $N_A/2$. Red dash: $|z\rangle|z\rangle \cdots$ at $(g_0, g_1) = (5\pi/16, 7\pi/16)$. Only at early times $t \leq N_A/4$ is there an exact linear ramp; beyond which the approach to maximum entropy becomes exponential.

which describe a 3-legged Kronecker delta with phase g and Hadamard respectively ($z_i \in \{0, 1\}$). Using standard rules of TN manipulations, we can build up the local gate $u(g_0, g_1)$ as shown in Fig. 1, and hence the global circuit U^t for time t (see [55] for details).

We find that U^t describes a *tiling of space-time by a decorated hexagonal lattice*. The diagrammatic representation makes immediately manifest that there are three ‘‘arrows of time’’, due to similarity of the tensor network under 120° rotations: perpendicular to any one of the black arrows in Fig. 1, the ‘‘evolution’’ of the circuit is unitary. This property can be termed ‘tri-unity’ [36], though we stress it is present at the global circuit level and not at the local gate level (there is no obvious ‘blocking’ of local gates to form a tri-unitary gate). We instead observe the local gates possess a recently-proposed relation governing contractions of pairs of them along the space direction, termed ‘‘second-level dual unitarity’’ (2DU) [37]:

$$\begin{array}{c} \text{---} \\ | \\ \text{---} \\ | \\ \text{---} \end{array} = \begin{array}{c} \text{---} \\ | \\ \text{---} \\ | \\ \text{---} \end{array}, \quad \begin{array}{c} \text{---} \\ | \\ \text{---} \\ | \\ \text{---} \end{array} = \begin{array}{c} \text{---} \\ | \\ \text{---} \\ | \\ \text{---} \end{array}, \quad (4)$$

which endows the system with analytic tractability in the computation of spatiotemporal correlations. Above, we have introduced bold tensors representing the folding of forward and backward branches of evolution, such as

$$\begin{array}{c} \text{---} \\ | \\ \text{---} \\ | \\ \text{---} \end{array} = \begin{array}{c} \text{---} \\ | \\ \text{---} \\ | \\ \text{---} \end{array}, \quad \text{---} = \cap, \quad (5)$$

which are the folded local gate $u \otimes u^*$ and trace operation respectively.

Importantly, while the discussion for the AKIM described a hexagonal lattice in (1+1)D, the idea behind its construction is quite general: for example, if instead we considered tiling of space-time with gates of Eq. (3) using a square lattice, then this describes a model with (standard) dual-unitary (two arrows of time, from the 90° rotation symmetry): the canonical self-dual kicked Ising model [24, 39]. However, one may repeat the same construction in higher spatial dimensions (see [38] too); further, the tiling of space-time need not be regular in flat space—for example, it could be a hyperbolic lattice (see e.g. [56, 57]). The construction extends too to systems of qudits through the natural qudit generalization of the phase and Hadamard gates, see the Supplemental Material [55]. Our proposal thus represents an appealing complementary geometrical picture to generate quantum circuits with generalized space-time duality like 2DU and possibly beyond.

Exact influence matrices.—We now return to the AKIM and demonstrate how its generalized space-time dual properties allow us to understand not only dynamics of few-point correlation functions (as was shown already in [36] and [37]), but also solve for its entanglement dynamics, which is much more complex. We note that because of its triunitary and 2DU properties, many aspects of its dynamics follow from [36, 37], but because of the model’s underlying geometric construction, it possesses additional structure allowing us to fully solve its dynamics under some conditions, as we shall see.

First, we note the RDM $\rho_A(t)$ can be computed by raising to a high power ‘spatial transfer matrices’ T , inserting the operator W mapping temporal information to the spatial region A , before tracing over the temporal degrees of freedom, see Fig. 2(a). Due to unitarity and locality of the original dynamics, it can be shown that T has only a single eigenvalue 1, with all other eigenvalues 0 with Jordan blocks bounded in size by $2t$, so that $T^{n \geq 2t} = |R\rangle\langle L|$, where $\langle L|, |R\rangle$ are the left and right eigenvectors respectively satisfying $\langle L|T = \langle L|$ and $T|R\rangle = |R\rangle$ [33, 53]. These eigenvectors are also called ‘influence matrices’ (IM), as they effectively encode the effect of the bath on the subsystem as a quantum state living on the temporal direction [33, 58, 59]. The computation of $\rho_A(t)$ in a thermodynamically large system thus simplifies to $\langle L|W|R\rangle$.

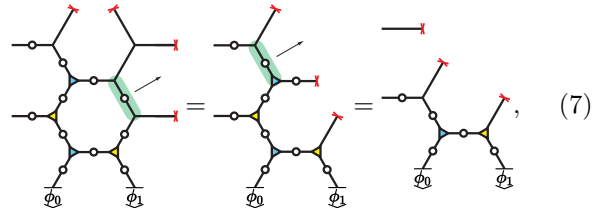
Generally, the form of an IM in a strongly-interacting system is complicated and has no closed form expression [58, 60, 61]. However, for the AKIM, if we impose that the dimerized product state $|\phi_0\rangle|\phi_1\rangle \cdots$ on B satisfies the *solvable IM conditions* (SIC):



$$\text{Diagram 1} = \frac{1}{q^2} \text{Diagram 2}, \quad \text{Diagram 3} = \frac{1}{q^2} \text{Diagram 4}, \quad (6)$$

we find $|L\rangle = |R\rangle$ and admits the simple form of a product of t Bell pairs, see Fig. 2(b) and [55]. This IM for

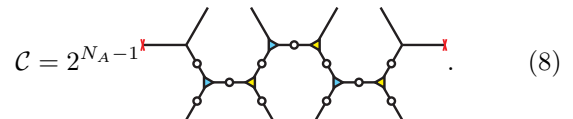
the AKIM is identical to that of dual-unitary circuits (within its corresponding solvable states [27]): it has zero temporal entanglement, such that the bath’s effect is a perfect Markovian dephaser on the boundaries. Proving this involves straightforward TN manipulations [55], for example deriving $T|R\rangle = |R\rangle$ for $t = 2$ proceeds as follows:



$$\text{Diagram 1} = \text{Diagram 2} = \text{Diagram 3}, \quad (7)$$

where we used unitarity along the black arrows to remove the green-shaded gates, before invoking SIC.

We thus establish our first result for the AKIM: the RDM can be computed exactly as $\rho_A(t) = \mathcal{C}^t [|\Psi\rangle_A \langle \Psi|_A]$ where the quantum channel \mathcal{C} is



$$\mathcal{C} = 2^{N_A - 1} \text{Diagram}, \quad (8)$$

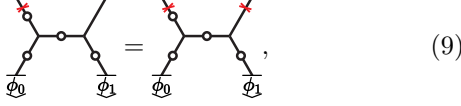
Note \mathcal{C} is unital: $\mathcal{C}[I_A] = I_A$, i.e., the infinite-temperature state $\rho_{T=\infty} = I_A/2^{N_A}$ is a steady-state, though there can be more. Physically, \mathcal{C} describes evolution under the AKIM on region A for one time-step, followed by dephasing on the boundaries. We emphasize this result amounts to a tremendous reduction of the complexity of the problem, as it entails an efficient $O(N^0)$ classical protocol to compute local dynamics even in a thermodynamically large system.

Solvable entanglement dynamics—Next, we consider entanglement entropy generation within A . We can divide the analysis into two cases: (i) early times $t \leq N/4$, when the TN factorizes into two disjoint diagrams due to causality; and (ii) late-times $t > N/4$.

For early times (i), for *any* (g_0, g_1) , we find that if states in A also satisfy SIC, then we can prove $S(t) = 2t$ which has also been independently obtained in parallel work [62]. Diagrammatically, this is done by fully contracting the shallow TN corresponding to the generalized purity $\text{tr}(\rho_A^n(t))$ for all $n \in \mathbb{N}$ and taking the limit $\lim_{n \rightarrow 1} S_n(t)$ where $S_n(t)$ is the n -th Rényi entropy [55].

For late-times (ii), we can further distinguish the following cases which go beyond the regime discussed in [62]. Case (a): when $g_0 = 0$ or π with arbitrary g_1 , we identify a set of local TN identities enabling us to prove $\mathcal{C}^{N_A+1} = \mathcal{C}^{N_A}$, and that $\rho_{T=\infty}$ is the only non-trivial eigenvector [55]. This implies *any* initial state $|\Psi\rangle$ thermalizes *exactly* to infinite-temperature in at most $t = N_A$. However, there are states which equilibrate faster: if dimerized product states on A satisfy SIC and addition-

ally *solvable entanglement conditions* (SEC):

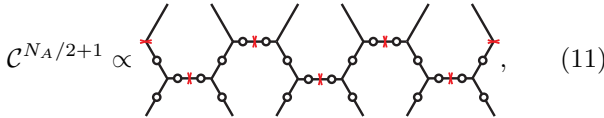


where the red cross is

$$\text{---}\times\text{---} = \left| \right\rangle\!\!\left. \right\rangle = \sum_z \frac{1}{z} \left| \begin{array}{c} z \\ z \\ z \\ z \end{array} \right\rangle, \quad (10)$$

a projector pinning the forwards and backwards branches into the same computational basis state, then provably $S(t) = \min(2t, N_A)$, see Fig. 2(c) [55]. These “maximum-entanglement-solvable” states are exhausted by $|\phi_0\rangle|\phi_1\rangle \in \{|z\rangle \otimes e^{i\theta X}|0\rangle\} \cup \{|\pm\rangle \otimes e^{i\theta Z}|+\rangle\}$, where $X|\pm\rangle = \pm|\pm\rangle$. We note the rate of entanglement generation is half the maximum possible in local brickwork circuits, achieved in dual-unitary circuits [63]. This is consistent with the results of recent work exploring quantum information propagation speeds in 2DU circuits [62] (here, their $n_A = d$, predicting an asymptotic entanglement velocity $v_E = 1/2$; however we stress our finding holds even non-asymptotically).

Case (b): when $g_0 = g_1 = \pi/2$, (or $3\pi/2$), instead another set of local TN identities hold so that $\mathcal{C}^{N_A/2+1} = \mathcal{C}^{N_A/2+2}$. This implies that system equilibrates exactly at finite time $t = N_A/2 + 1$ for a generic state. However, interestingly, $\rho_{T=\infty}$ is now not the only steady-state — the equilibrium state need not have maximal entropy. To understand what the additional steady-states are, we show in [55] the late-time channel has the TN



and read-off that $\mathcal{C}^{N_A/2+1} = b_1 \circ b_{N_A} \circ \prod_{\text{even bonds}} c_{i,i+1} \circ \prod_{\text{odd bonds}} d_{i,i+1}$, where b_i is the local Z -dephasing channel, and $c(d)_{i,i+1}$ are the two-site $ZZ(XX)$ -dissipative channels. For example, $c_{i,i+1}[\rho] = \frac{1}{2}(\rho + Z_i Z_{i+1} \rho Z_i Z_{i+1})$. It is straightforward to check there is a super-extensive set of 2^{N_A-1} independent operators invariant under \mathcal{C} , given by all products of $Z_i Z_{i+1}$ on odd bonds and $X_i X_{i+1}$ on even bonds. Focusing on the family of dimerized initial states $|\phi_0\rangle|\phi_1\rangle \in \{|z\rangle \otimes e^{i\theta Z}|+\rangle\} \cup \{|y, \pm\rangle \otimes e^{i\phi X}|0\rangle\}$ and those related by $\phi_0 \leftrightarrow \phi_1$ (here $Y|y, \pm\rangle = \pm|y, \pm\rangle$), we can show that these states have zero expectation values within the conserved quantities and moreover have exact linear growth of entanglement $S(t) = \min(2t, N_A)$. We dub these “maximum-entanglement-solvable” states too. For $|z\rangle|z\rangle \dots$ instead $S(t) = \min(2t, N_A/2)$. These are illustrated in Fig. 2(c).

Case (c): when $(g_0, g_1) = (\pi/2, 3\pi/2)$, the situation is richer as we find \mathcal{C} has now some eigenvectors with

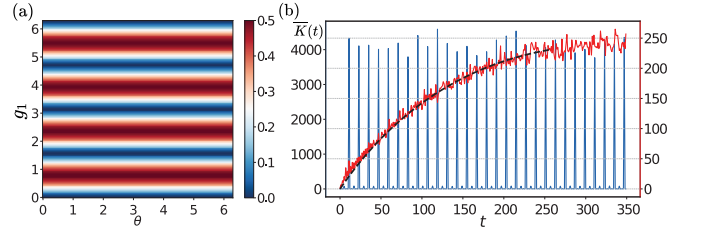


FIG. 3. (a) Operator entanglement of a stabilizer at intermediate times underpinning the RDM $\rho_A(t)$, as a function of phase g_1 and angle θ parameterizing the initial state. The stabilizer generally has non-trivial operator entanglement entropy, indicating complex structure in space that cannot be exhibited by Pauli stabilizers. (b) SFF of the AKIM at $N_A = 8$. Blue (left y-axis): SFF for $g_0 = 0$, shows regular revivals. Red (right y-axis): SFF for generic parameters falls within the COE class: the fit is to the RMT prediction $2t - t \ln(1 + 2t/2^{N_A})$ [64]. Note the differences in scale.

eigenvalue -1 , indicating that the system generically does not equilibrate but rather oscillates at late times! This stems from the facts that (i) states satisfying SIC at $(\pi/2, \pi/2)$ are identical to those at $(\pi/2, 3\pi/2)$, and (ii) the action of the channel in the latter case (called $\mathcal{C}_{1/2,3/2}$) applied t times is equal to that of the former (called $\mathcal{C}_{1/2,1/2}$) applied t times, followed by the action of a Pauli channel which cycles between $IYIY \dots, YYY Y, \dots, YIYI \dots, IIII \dots$ beginning at $t = 1$. This arises from the circuits’ Clifford nature [55]. Since we know the invariant operators of $\mathcal{C}_{1/2,1/2}^t$ at late times ($t \geq N_A/2 + 1$), which all commute with $Y Y Y Y \dots$ but not all with $IYIY \dots$ or $YIYI \dots$, it follows that $\mathcal{C}_{1/2,3/2}^t = \mathcal{C}_{1/2,1/2}^t$ and $\mathcal{P}_{IY} \circ \mathcal{C}_{1/2,1/2}^t$ for late even and odd t respectively, explaining the generic oscillatory behavior. However, since a Pauli channel is non-entangling, entanglement dynamics at $(\pi/2, \pi/2)$ and $(\pi/2, 3\pi/2)$ will be identical for the same state.

Lastly, for generic (g_0, g_1) away from cases (a-c), we numerically find $\rho_{T=\infty}$ is the unique unity eigenvector of \mathcal{C} , while there are eigenvectors with non-zero eigenvalues λ . The spectral gap $\Delta := 1 - \max_{\lambda: |\lambda| < 1} |\lambda|$ determines the rate of thermalization (see [55] for a numerical analysis). We also do not find any obvious simple product states whose entanglement dynamics can be analytically understood beyond the early-time regime (Fig. 2(c)).

Discussion.—We have introduced the AKIM, and through it demonstrated a general geometrical construction of quantum circuits possessing generalized space-time duality via the idea of space-time tiling. This construction recovers existing space-time dualities, like dual-unitarity [24–29] and second level dual-unitarity [37]. For the AKIM, we further showed how because of its generalized space-time dual properties, its entanglement dynamics can be efficiently and at times fully solved.

It is interesting to contrast our findings to other known analytically-solvable models of quantum dynamics. To

the best of our knowledge, our model is not generically integrable nor Clifford (namely, dynamics which preserve the Pauli group [20–23]). However, our calculation of the generalized purities in the entanglement solvable cases (a) $g_0 = 0$ or π with arbitrary g_1 , (b) $g_0 = g_1 = \pi/2$ or $3\pi/2$, (c) $g_0 = \pi/2$ and $g_1 = 3\pi/2$ yields that the entanglement spectrum of $\rho_A(t)$ is flat [55], a feature exhibited too by Clifford dynamics beginning from stabilizer states [21]. On the other hand, we find that only parameters $(g_0, g_1) = (n\pi/2, m\pi/2)$ of the AKIM where $n, m \in \mathbb{Z}$, constitute Clifford circuits, while we have shown that full entanglement-solvability extends beyond these isolated points — namely, a large parameter range within case (a). Moreover, even when the AKIM is Clifford, as in case (b,c) and specific points in case (a), the entanglement-solvable states need *not* be stabilizer states, a condition otherwise needed in order for the Gottesman-Knill theorem of efficient classical simulability to apply [20, 65]. Thus, solvability in these cases does not seem tied to the circuit being Clifford.

To drive home the difference of the entanglement solvable cases of the AKIM with Clifford evolution, we investigate the decomposition of the RDM at various times for case (a): $g_0 = 0$ and arbitrary g_1 , beginning from dimerized initial states $|0\rangle \otimes e^{i\theta X}|0\rangle$ on A , into the product of projectors onto orthogonal eigenspaces $\rho_A(t) \propto \prod_i (1 + O_i)$. Here the stabilizers O_i are defined to be mutually commuting, each having equal numbers of ± 1 eigenvalues, but need not be a Pauli string. Fig. 3(a) shows a characterization of the spatial structure of a representative O_i at a later time: it generically develops operator entanglement—entropy related to non-factorizability into a tensor product of locally-supported operators (details in [55]), which can never happen under Clifford evolution [20, 66]. Moreover, the spectral form factor (SFF) $\bar{K}(t) = |\text{tr}(U^t)|^2$ [24, 67] for $g_0 = 0$ (averaging over spatially-random g_1 uniformly [68]), exhibits surprisingly large, apparently time-quasiperiodic revivals, which conforms neither to Poissonian, Wigner-Dyson dynamical classes, nor those of Clifford circuits (see e.g. [22]). To the best of our knowledge, this represents an interesting new kind of non-chaotic yet non-integrable, non-Clifford quantum dynamics deserving further investigation. In contrast, uniformly averaging over g_0, g_1 yields an SFF agreeing perfectly with the circular orthogonal ensemble (COE) of random matrix theory (RMT) [64]. All these indicate that the physics of the AKIM is very rich. It would be interesting to analyze the dynamics of other generalized space-time dual models, generated similarly from the geometric construction we have put forth in this work.

Acknowledgments. We thank Katja Klobas, Bruno Bertini and Huang Qi for interesting discussions. W. W. H. is supported by the Singapore NRF Fellowship, NRF-NRFF15-2023-0008, and the CQT Bridging Fund.

* c.liu@u.nus.edu

† wenweiho@nus.edu.sg

- [1] Marcos Rigol, Vanja Dunjko, and Maxim Olshanii, “Thermalization and its mechanism for generic isolated quantum systems,” *Nature* **452**, 854–858 (2008).
- [2] Rahul Nandkishore and David A. Huse, “Many-body localization and thermalization in quantum statistical mechanics,” *Annual Review of Condensed Matter Physics* **6**, 15–38 (2015).
- [3] Luca D’Alessio, Yariv Kafri, Anatoli Polkovnikov, and Marcos Rigol, “From quantum chaos and eigenstate thermalization to statistical mechanics and thermodynamics,” *Advances in Physics* **65** (2016), 10.1080/00018732.2016.1198134.
- [4] Dmitry A. Abanin, Ehud Altman, Immanuel Bloch, and Maksym Serbyn, “Colloquium: Many-body localization, thermalization, and entanglement,” *Rev. Mod. Phys.* **91**, 021001 (2019).
- [5] Patrick Hayden and John Preskill, “Black holes as mirrors: quantum information in random subsystems,” *Journal of High Energy Physics* **2007**, 120–120 (2007).
- [6] Stephen H. Shenker and Douglas Stanford, “Black holes and the butterfly effect,” *Journal of High Energy Physics* **2014**, 67 (2014).
- [7] Pavan Hosur, Xiao-Liang Qi, Daniel A. Roberts, and Beni Yoshida, “Chaos in quantum channels,” *J. High Energy Phys.* **2**, 4 (2016).
- [8] Daniel A. Roberts and Beni Yoshida, “Chaos and complexity by design,” *Journal of High Energy Physics* **2017**, 121 (2017).
- [9] Mark Mezei and Douglas Stanford, “On entanglement spreading in chaotic systems,” *Journal of High Energy Physics* **2017**, 65 (2017).
- [10] K. A. Landsman, C. Figgatt, T. Schuster, N. M. Linke, B. Yoshida, N. Y. Yao, and C. Monroe, “Verified quantum information scrambling,” *Nature* **567**, 61–65 (2019).
- [11] Hideo Aoki, Naoto Tsuji, Martin Eckstein, Marcus Kollar, Takashi Oka, and Philipp Werner, “Nonequilibrium dynamical mean-field theory and its applications,” *Rev. Mod. Phys.* **86**, 779–837 (2014).
- [12] Guifré Vidal, “Efficient classical simulation of slightly entangled quantum computations,” *Phys. Rev. Lett.* **91**, 147902 (2003).
- [13] A J Daley, C Kollath, U Schollwöck, and G Vidal, “Time-dependent density-matrix renormalization-group using adaptive effective hilbert spaces,” *Journal of Statistical Mechanics: Theory and Experiment* **2004**, P04005 (2004).
- [14] Sebastian Paeckel, Thomas Köhler, Andreas Swoboda, Salvatore R. Manmana, Ulrich Schollwöck, and Claudius Hubig, “Time-evolution methods for matrix-product states,” *Annals of Physics* **411**, 167998 (2019).
- [15] Kévin Hémerly, Frank Pollmann, and David J. Luitz, “Matrix product states approaches to operator spreading in ergodic quantum systems,” *Phys. Rev. B* **100**, 104303 (2019).
- [16] Vincenzo Alba and Pasquale Calabrese, “Entanglement and thermodynamics after a quantum quench in integrable systems,” *Proceedings of the National Academy of Sciences* **114**, 7947–7951 (2017).
- [17] Fabian H L Essler and Maurizio Fagotti, “Quench dy-

- namics and relaxation in isolated integrable quantum spin chains,” *Journal of Statistical Mechanics: Theory and Experiment* **2016**, 064002 (2016).
- [18] Pasquale Calabrese, “Entanglement spreading in non-equilibrium integrable systems,” *SciPost Physics Lecture Notes*, 20 (2020).
- [19] Katja Klobas, Bruno Bertini, and Lorenzo Piroli, “Exact thermalization dynamics in the “rule 54” quantum cellular automaton,” *Phys. Rev. Lett.* **126**, 160602 (2021).
- [20] Michael A. Nielsen and Isaac L. Chuang, *Quantum Computation and Quantum Information* (Cambridge University Press, Cambridge, 2000).
- [21] Adam Nahum, Jonathan Ruhman, Sagar Vijay, and Jeongwan Haah, “Quantum entanglement growth under random unitary dynamics,” *Phys. Rev. X* **7**, 031016 (2017).
- [22] Tom Farshi, Jonas Richter, Daniele Toniolo, Arijeet Pal, and Lluís Masanes, “Absence of localization in two-dimensional clifford circuits,” *PRX Quantum* **4**, 030302 (2023).
- [23] Jonas Richter, Oliver Lunt, and Arijeet Pal, “Transport and entanglement growth in long-range random clifford circuits,” *Phys. Rev. Res.* **5**, L012031 (2023).
- [24] Bruno Bertini, Pavel Kos, and Tomaz Prosen, “Exact spectral form factor in a minimal model of many-body quantum chaos,” *Phys. Rev. Lett.* **121**, 264101 (2018).
- [25] Sarang Gopalakrishnan and Austen Lamacraft, “Unitary circuits of finite depth and infinite width from quantum channels,” *Phys. Rev. B* **100**, 064309 (2019).
- [26] Suhail Ahmad Rather, S. Aravinda, and Arul Lakshminarayan, “Creating ensembles of dual unitary and maximally entangling quantum evolutions,” *Phys. Rev. Lett.* **125**, 070501 (2020).
- [27] Lorenzo Piroli, Bruno Bertini, J. Ignacio Cirac, and Tomaz Prosen, “Exact dynamics in dual-unitary quantum circuits,” *Phys. Rev. B* **101**, 094304 (2020).
- [28] Pieter W. Claeys and Austen Lamacraft, “Ergodic and nonergodic dual-unitary quantum circuits with arbitrary local hilbert space dimension,” *Phys. Rev. Lett.* **126**, 100603 (2021).
- [29] Ana Flack, Bruno Bertini, and Tomaz Prosen, “Statistics of the spectral form factor in the self-dual kicked ising model,” *Phys. Rev. Res.* **2**, 043403 (2020).
- [30] M. C. Bañuls, M. B. Hastings, F. Verstraete, and J. I. Cirac, “Matrix product states for dynamical simulation of infinite chains,” *Phys. Rev. Lett.* **102**, 240603 (2009).
- [31] M. B. Hastings and R. Mahajan, “Connecting entanglement in time and space: Improving the folding algorithm,” *Phys. Rev. A* **91**, 032306 (2015).
- [32] Bruno Bertini, Pavel Kos, and Tomaz Prosen, “Entanglement spreading in a minimal model of maximal many-body quantum chaos,” *Phys. Rev. X* **9**, 021033 (2019).
- [33] Alessio Lerose, Michael Sonner, and Dmitry A. Abanin, “Influence matrix approach to many-body floquet dynamics,” *Phys. Rev. X* **11**, 021040 (2021).
- [34] Tsung-Cheng Lu and Tarun Grover, “Spacetime duality between localization transitions and measurement-induced transitions,” *PRX Quantum* **2**, 040319 (2021).
- [35] Matteo Ippoliti, Tibor Rakovszky, and Vedika Khemani, “Fractal, logarithmic, and volume-law entangled non-thermal steady states via spacetime duality,” *Phys. Rev. X* **12**, 011045 (2022).
- [36] Cheryne Jonay, Vedika Khemani, and Matteo Ippoliti, “Triunitary quantum circuits,” *Phys. Rev. Res.* **3**, 043046 (2021).
- [37] Xie-Hang Yu, Zhiyuan Wang, and Pavel Kos, “Hierarchical generalization of dual unitarity,” *Quantum* **8**, 1260 (2024).
- [38] Vladimir Al. Osipov, Niclas Krieger, Thomas Guhr, and Boris Gutkin, “Local correlations in partially dual-unitary lattice models,” *Phys. Rev. B* **109**, 214302 (2024).
- [39] Wen Wei Ho and Soonwon Choi, “Exact emergent quantum state designs from quantum chaotic dynamics,” *Phys. Rev. Lett.* **128**, 060601 (2022).
- [40] Jordan S. Cotler, Daniel K. Mark, Hsin-Yuan Huang, Felipe Hernández, Joonhee Choi, Adam L. Shaw, Manuel Endres, and Soonwon Choi, “Emergent quantum state designs from individual many-body wave functions,” *PRX Quantum* **4**, 010311 (2023).
- [41] Matteo Ippoliti and Wen Wei Ho, “Solvable model of deep thermalization with distinct design times,” *Quantum* **6**, 886 (2022).
- [42] Matteo Ippoliti and Wen Wei Ho, “Dynamical purification and the emergence of quantum state designs from the projected ensemble,” *PRX Quantum* **4**, 030322 (2023).
- [43] Harshank Shrotriya and Wen Wei Ho, “Nonlocality of deep thermalization,” (2023), arXiv:2305.08437 [quant-ph].
- [44] Mark Srednicki, “Chaos and quantum thermalization,” *Physical Review E* **50**, 888–901 (1994).
- [45] Amos Chan, Andrea De Luca, and J. T. Chalker, “Solution of a minimal model for many-body quantum chaos,” *Phys. Rev. X* **8**, 041019 (2018).
- [46] Brian Skinner, Jonathan Ruhman, and Adam Nahum, “Measurement-induced phase transitions in the dynamics of entanglement,” *Phys. Rev. X* **9**, 031009 (2019).
- [47] Yaodong Li, Xiao Chen, and Matthew P. A. Fisher, “Measurement-driven entanglement transition in hybrid quantum circuits,” *Phys. Rev. B* **100**, 134306 (2019).
- [48] Soonwon Choi, Yimu Bao, Xiao-Liang Qi, and Ehud Altman, “Quantum error correction in scrambling dynamics and measurement-induced phase transition,” *Phys. Rev. Lett.* **125**, 030505 (2020).
- [49] Yimu Bao, Soonwon Choi, and Ehud Altman, “Theory of the phase transition in random unitary circuits with measurements,” *Phys. Rev. B* **101**, 104301 (2020).
- [50] Michael J. Gullans and David A. Huse, “Scalable probes of measurement-induced criticality,” *Phys. Rev. Lett.* **125**, 070606 (2020).
- [51] Pieter W. Claeys, Marius Henry, Jamie Vicary, and Austen Lamacraft, “Exact dynamics in dual-unitary quantum circuits with projective measurements,” *Phys. Rev. Res.* **4**, 043212 (2022).
- [52] Bruno Bertini, Pavel Kos, and Tomaz Prosen, “Localized dynamics in the floquet quantum east model,” *Phys. Rev. Lett.* **132**, 080401 (2024).
- [53] Bruno Bertini, Cecilia De Fazio, Juan P. Garrahan, and Katja Klobas, “Exact quench dynamics of the floquet quantum east model at the deterministic point,” *Phys. Rev. Lett.* **132**, 120402 (2024).
- [54] Nicola Pancotti, Giacomo Giudice, J. Ignacio Cirac, Juan P. Garrahan, and Mari Carmen Bañuls, “Quantum east model: Localization, nonthermal eigenstates, and slow dynamics,” *Phys. Rev. X* **10**, 021051 (2020).
- [55] See Supplemental material online for details of tensor network notation and manipulation, as well as proofs of statements presented in the main text.

- [56] Alicia J. Kollár, Mattias Fitzpatrick, and Andrew A. Houck, “Hyperbolic lattices in circuit quantum electrodynamics,” *Nature* **571**, 45–50 (2019).
- [57] Przemyslaw Bienias, Igor Boettcher, Ron Belyansky, Alicia J. Kollár, and Alexey V. Gorshkov, “Circuit quantum electrodynamics in hyperbolic space: From photon bound states to frustrated spin models,” *Phys. Rev. Lett.* **128**, 013601 (2022).
- [58] Michael Sonner, Alessio Lerose, and Dmitry A. Abanin, “Influence functional of many-body systems: Temporal entanglement and matrix-product state representation,” *Annals of Physics* **435**, 168677 (2021), special issue on Philip W. Anderson.
- [59] Giacomo Giudice, Giuliano Giudici, Michael Sonner, Julian Thoenniss, Alessio Lerose, Dmitry A. Abanin, and Lorenzo Piroli, “Temporal entanglement, quasiparticles, and the role of interactions,” *Phys. Rev. Lett.* **128**, 220401 (2022).
- [60] Alessio Lerose, Michael Sonner, and Dmitry A. Abanin, “Scaling of temporal entanglement in proximity to integrability,” *Phys. Rev. B* **104**, 035137 (2021).
- [61] Alessandro Foligno, Tianci Zhou, and Bruno Bertini, “Temporal entanglement in chaotic quantum circuits,” *Phys. Rev. X* **13**, 041008 (2023).
- [62] Alessandro Foligno, Pavel Kos, and Bruno Bertini, “Quantum information spreading in generalized dual-unitary circuits,” *Phys. Rev. Lett.* **132**, 250402 (2024).
- [63] Tianci Zhou and Aram W. Harrow, “Maximal entanglement velocity implies dual unitarity,” *Phys. Rev. B* **106**, L201104 (2022).
- [64] M. L. Mehta, *Random Matrices and the Statistical Theory of Spectra*, 2nd ed. (Academic, New York, 1991).
- [65] Daniel Gottesman, “The heisenberg representation of quantum computers,” arXiv:quant-ph/9807006 (1998).
- [66] David Fattal, Toby S. Cubitt, Yoshihisa Yamamoto, Sergey Bravyi, and Isaac L. Chuang, “Entanglement in the stabilizer formalism,” (2004), arXiv:quant-ph/0406168 [quant-ph].
- [67] Junyu Liu, “Spectral form factors and late time quantum chaos,” *Phys. Rev. D* **98**, 086026 (2018).
- [68] We note each instance of the circuit from this ensemble has entanglement dynamics which is still analytically solvable.

Supplemental Information: Solvable entanglement dynamics in quantum circuits with generalized space-time duality

Chuan Liu^{1,*} and Wen Wei Ho^{1,2,†}

¹*Department of Physics, National University of Singapore, Singapore 117542*

²*Centre for Quantum Technologies, National University of Singapore, 3 Science Drive 2, Singapore 117543*

In this supplemental information, we provide details on the tensor network (TN) analysis of the alternating kicked Ising model (AKIM) for systems of qudits with arbitrary local Hilbert space dimension, proofs of various statements on entanglement dynamics, as well as numerical investigations into the properties of the channel \mathcal{C} governing local dynamics and the fine-structure of stabilizers under entanglement-solvable dynamics.

Concretely, Sec. I describes the connection of the AKIM to the deterministic Floquet quantum East Model (DFQE). Sec. II presents the tensor network framework in which the analysis of the AKIM is performed in. Sec. III derives the fixed points of the spatial transfer matrix considered in the main text, i.e., the influence matrices (IM), as well as the structure of initial states satisfying the solvable influence-matrix conditions (SIC). Sec. IV derives the general result of exact early-time ($t \leq N_A/4$) entanglement dynamics for dimerized initial states satisfying the SIC. Sec. V focuses on entanglement dynamics of the AKIM with $\vec{g}_0 = \vec{0}$ and arbitrary \vec{g}_1 , in particular on the maximum-entanglement-solvable states. Sec. VI describes the entanglement dynamics of the AKIM on qubits at parameter regimes harboring degenerate steady-states (this is given by $g_0 = (2n+1)\pi/2$, $g_1 = (2m+1)\pi/2$, with $n, m \in \mathbb{Z}$). Sec. VII explores numerically the gap of the channel \mathcal{C} governing thermalizing dynamics of a local region, which sets the rate of thermalization. Sec. VIII investigates the spatial structure of stabilizers underlying the reduced density matrix arising in dynamics from maximum-entanglement-solvable states, in particular probing their operator entanglement entropy.

I. RELATION TO THE DETERMINISTIC FLOQUET QUANTUM EAST MODEL

Here, we illustrate the connection of the AKIM (on qubits) to the deterministic Floquet quantum East model [1, 2] (DFQE), whose entanglement dynamics was recently solved by [2]. It is an example of a kinetically constrained model, and is given as a brickwork circuit with two-local gates acting on a chain of qubits:

$$w = \mathbb{I} \otimes \bar{P} + X \otimes P, \quad (1)$$

where the projector $P = \mathbb{I} - \bar{P} = (\mathbb{I} + Z)/2$. The action of the gate is as such: when the control (right qubit) is in state $|0\rangle$, the target (left qubit) is left unchanged; while if the control is in $|1\rangle$, the target is flipped ($|z\rangle \rightarrow X|z\rangle$, where $z = 0, 1$). In other words, w is a CNOT gate.

The two-local gates we introduced in the main text,

$$u(g_0, g_1) = (P(g_0) \otimes P(g_1))CZ(H \otimes H), \quad (2)$$

are related to w via

$$w = (H \otimes I)u(0, 0)(\mathbb{I} \otimes H). \quad (3)$$

Thus, the two global circuits (AKIM and DFQE) are unitarily related by a tensor product of local unitaries:

$$U_{\text{DFQE}}^t = (\cdots \mathbb{I} \otimes H \otimes \mathbb{I} \otimes H \cdots) U_{\text{AKIM}}^t(g_0 = g_1 = 0) (\cdots \mathbb{I} \otimes H \otimes \mathbb{I} \otimes H \cdots), \quad (4)$$

implying that the entanglement dynamics of state $|\Psi\rangle$ under the DFQE and $(\cdots \mathbb{I} \otimes H \otimes \mathbb{I} \otimes H \cdots)|\Psi\rangle$ under the AKIM (at $g_0 = g_1 = 0$) are identical.

* c.liu@u.nus.edu

† wenweiho@nus.edu.sg

II. TENSOR NETWORK REPRESENTATION OF AKIM

A. Basic TN diagrams

In this section, we introduce the general tensor network notation used to analyze the circuit generated by the AKIM in arbitrary local qudit dimensions q (the main text focused on the qubit case). We note the AKIM can be always written as a Hamiltonian using clock and shift operators acting on a q -dimensional local space (defined below), which are the generalization of Pauli qubit operators, but we leave the explicit form as an exercise to the reader. The two basic tensors which form the building blocks of the quantum circuit are:

$$\begin{array}{c} z_2 \\ \diagdown \\ \vec{g} \\ \diagup \\ z_1 \end{array} \text{---} z_3 = \delta_{z_1 z_2 z_3} e^{ig^{(z_1)}}, \quad \begin{array}{c} z_2 \\ | \\ \circ \\ | \\ z_1 \end{array} := H_{z_1 z_2} = \frac{1}{\sqrt{q}} \omega^{z_1 z_2}. \quad (5)$$

The first tensor has three legs and is labeled by a q -dimensional vector $\vec{g} = (1, g^{(1)}, g^{(2)}, \dots, g^{(q-1)})$, and denotes a generalized Kronecker-delta function $\delta_{z_1 z_2 z_3} e^{ig^{(z_1)}}$ which enforces all inputs to be equal in the computational basis $z = 0, 1, \dots, q-1$, upon which it evaluates to the phase $e^{ig^{(z_1)}}$, otherwise it vanishes. The second tensor is the quantum Fourier transform operator, with matrix elements in the computational basis given by the discrete Fourier transform matrix $H_{z_1 z_2} = \frac{1}{\sqrt{q}} \omega^{z_1 z_2}$ where $\omega = e^{i2\pi/q}$. When $q = 2$ (qubit), this reduces to the familiar Hadamard matrix $H = \frac{1}{\sqrt{2}} \begin{pmatrix} 1 & 1 \\ 1 & -1 \end{pmatrix}$.

We will also find it useful to introduce tensors denoting the q -dimensional clock and shift operators respectively,

$$\begin{array}{c} z_2 \\ | \\ \boxed{Z}^j \\ | \\ z_1 \end{array} := Z_{z_1 z_2}^j = \delta_{z_1 z_2} \omega^{z_1 j}, \quad \begin{array}{c} z_2 \\ | \\ \boxed{X}^j \uparrow \\ | \\ z_1 \end{array} := X_{z_1 z_2}^j = \begin{cases} 0, & z_2 \equiv z_1 + j \pmod{q} \\ 1, & z_2 \not\equiv z_1 + j \pmod{q} \end{cases} \quad (6)$$

Above, j denotes the integer power that the operator is raised to, and is not an index. Note that because the shift operator X is not symmetric in general (i.e., $X^T \neq X$), we have also drawn an arrow in the diagram for X to denote the direction of its right action. For quantum states, their TN representation is simply

$$\frac{1}{\sqrt{q}} := |\phi_1\rangle. \quad (7)$$

Following standard TN rules on contracting tensors (one can join tensors by connecting legs and summing over the underlying indices), we can produce derivative tensors. For example, we can compute the following diagram

$$u(\vec{g}_0, \vec{g}_1) = \sqrt{q} \begin{array}{c} \diagdown \quad \diagup \\ \vec{g}_0 \quad \vec{g}_1 \\ \diagup \quad \diagdown \\ \circ \quad \circ \end{array} = (P(\vec{g}_0) \otimes P(\vec{g}_1)) CZ(H \otimes H), \quad (8)$$

which describes the two-local qudit gate $u(\vec{g}_0, \vec{g}_1)$ that builds up the brickwork circuit of the AKIM. Here, $CZ := \text{diag}(\underbrace{1, 1, \dots, 1}_q, \underbrace{1, \omega, \dots, \omega^{q-1}}_q, \dots, \underbrace{1, \omega^{q-1}, \dots, \omega^{q(q-1)}}_q)$ and $P(\vec{g}_i) := \text{diag}(1, e^{ig_i^{(1)}}, e^{ig_i^{(2)}}, \dots, e^{ig_i^{(q-1)}})$ are the generalized control-Z and phase gates respectively, for qudits. In the qubit case, this reduces to the familiar $CZ = \text{diag}(1, 1, 1, -1)$ and $P(g_i) = \text{diag}(1, e^{ig_i})$.

B. TN in folded representation

In the study of quantum dynamics, we routinely consider objects like $|\Psi(t)\rangle = U(t)|\Psi(0)\rangle \langle\Psi(0)|U(t)^\dagger$ and $\rho_A(t) = \text{tr}_B |\Psi(t)\rangle \langle\Psi(t)|$. We see that this always involves the forwards and backwards branches of time-evolution together (and more pairs of forwards and backwards branches if we are computing, say, the entanglement entropy). It is convenient to vectorize the adjoint map $U[\cdot]U^\dagger$ into a matrix acting on a doubled Hilbert space $U \otimes U^*$, which

amounts to ‘folding’ U^\dagger into U^* , as well as vectorize the quantum state $|\phi\rangle\langle\phi| \mapsto |\phi\rangle \otimes |\phi\rangle^*$. To represent these in TN notation, we introduce bold tensors, for example of the local gates and local states $u \otimes u^*$ and $|\phi_1\rangle \otimes |\phi_1\rangle^*$

$$\text{Diagrammatic equation (9)} \quad (9)$$

Then the trace operation (on one qubit) and the projector $\sum_z |zz\rangle\langle zz|$ pinning forwards and backwards branches (which will routinely show up) can be diagrammatically represented as

$$\text{Diagrammatic equation (10)} \quad (10)$$

Using these bold folded tensors, we can carry out diagrammatic calculations very compactly. For example the unitarity of the gates Eq. (8) can be expressed

$$\text{Diagrammatic equation (11)} \quad (11)$$

which represents $u^\dagger u = \mathbb{I}$ (in unfolded language), while

$$\text{Diagrammatic equation (12)} \quad (12)$$

represents $uu^\dagger = \mathbb{I}$. Another example is the overlap of states (assumed normalized)

$$\text{Diagrammatic equation (13)} \quad (13)$$

and the following will be extremely useful relations that we will routinely employ:

$$\text{Diagrammatic equation (14)} \quad (14)$$

III. TRANSFER MATRIX AND INFLUENCE MATRICES

Here we provide additional details on the assertion in the main text that the influence matrices (both left and right) are a product of t Bell states, assuming that the system on B is prepared in a dimerized product state $\prod_i |\phi_0\rangle_{2i-1} |\phi_1\rangle_{2i}$ which satisfies the *Solvable Influence-matrix Conditions* (SIC):

$$\text{Diagrammatic equation (15)} \quad (15)$$

Now, the right and left influence matrices $|R\rangle$ and $\langle L|$ are defined to be the unique (unique due to unitarity of the

original circuit) right and left eigenvector of T with unit eigenvalue [3], i.e., $T|R\rangle = |R\rangle$ and $\langle L|T = \langle L|$, where

$$T = q^{2t} \quad (16)$$

Note that it can also be shown all other eigenvalues of T are zero and its largest Jordan block is of size $2t$ because of locality of the dynamics (see [2, 3]). Our claim is that for the AKIM with states satisfying SIC on B ,

$$|R\rangle = \begin{matrix} \text{---} \times \\ \text{---} \times \\ \text{---} \times \\ \text{---} \times \end{matrix}, \quad \langle L| = \begin{matrix} \times \text{---} \\ \times \text{---} \\ \times \text{---} \\ \times \text{---} \end{matrix}. \quad (17)$$

Notice that $|L\rangle = |R\rangle$.

This can be proven straightforwardly, diagrammatically. We compute:

$$T|R\rangle = q^{2t} = q^{2t} = q^{t+1} = q^2 \begin{matrix} \text{---} \times \\ \text{---} \times \\ \text{---} \times \\ \text{---} \times \end{matrix} = \begin{matrix} \text{---} \times \\ \text{---} \times \\ \text{---} \times \\ \text{---} \times \end{matrix}, \quad (18)$$

where in the third and fourth equality, we continually use the triunitary/generalized dual-unitary property in the time direction represented by the arrows, to remove green shaded boxes (since it is unitary in that direction), while in the

last equality, we utilized SIC. Similarly, using generalized dual-unitarity and SIC we can compute

$$\langle L|T = q^{2t} = q^{2t} = q^{t+1} = q^2 \quad (19)$$

Given these influence matrices, the reduced density matrix for subsystem A deep inside the bulk then takes a simple form:

$$\rho_A(t) = q^{t(N_A - 1)} \quad (20)$$

and we see that it can be obtained by iterating the following quantum channel \mathcal{C} :

$$\mathcal{C} = q^{N_A - 1} \quad (21)$$

on the initial state $|\Psi\rangle\langle\Psi|$. This quantum channel is a composition of a unitary channel describing time-evolution by the AKIM in region A , as well as a channel describing z -dephasing on the boundaries.

A. Solving the SICs

We show here that there are non-trivial solutions to the SICs. Explicitly, the SICs imply:

$$\delta_{ij} = \begin{array}{c} |j\rangle^\dagger \\ \text{---} \\ |i\rangle \end{array} = q^2 \begin{array}{c} \widehat{\phi}_0^\dagger \quad \widehat{\phi}_1^\dagger \\ \text{---} \\ \text{---} \\ \text{---} \\ \phi_0 \quad \phi_1 \end{array} = q \begin{array}{c} \widehat{\phi}_0^\dagger \quad \widehat{\phi}_1^\dagger \\ \text{---} \\ \text{---} \\ \text{---} \\ \phi_0 \quad \phi_1 \end{array} \\
= q \begin{array}{c} \widehat{\phi}_0^\dagger \quad \widehat{\phi}_1^\dagger \\ \text{---} \\ \text{---} \\ \text{---} \\ \phi_0 \quad \phi_1 \end{array} = q \begin{array}{c} \widehat{\phi}_0^\dagger \quad \widehat{\phi}_1^\dagger \\ \text{---} \\ \text{---} \\ \text{---} \\ \phi_0 \quad \phi_1 \end{array} = q \begin{array}{c} \widehat{\phi}_0^\dagger \quad \widehat{\phi}_1^\dagger \\ \text{---} \\ \text{---} \\ \text{---} \\ \phi_0 \quad \phi_1 \end{array} \quad (22)$$

$$\delta_{ij} = \begin{array}{c} |j\rangle^\dagger \\ \text{---} \\ |i\rangle \end{array} = q^2 \begin{array}{c} \widehat{\phi}_0^\dagger \quad \widehat{\phi}_1^\dagger \\ \text{---} \\ \text{---} \\ \text{---} \\ \phi_0 \quad \phi_1 \end{array} = q \begin{array}{c} \widehat{\phi}_0^\dagger \quad \widehat{\phi}_1^\dagger \\ \text{---} \\ \text{---} \\ \text{---} \\ \phi_0 \quad \phi_1 \end{array} \\
= q \begin{array}{c} \widehat{\phi}_0^\dagger \quad \widehat{\phi}_1^\dagger \\ \text{---} \\ \text{---} \\ \text{---} \\ \phi_0 \quad \phi_1 \end{array} = q \begin{array}{c} \widehat{\phi}_0^\dagger \quad \widehat{\phi}_1^\dagger \\ \text{---} \\ \text{---} \\ \text{---} \\ \phi_0 \quad \phi_1 \end{array} = q \begin{array}{c} \widehat{\phi}_0^\dagger \quad \widehat{\phi}_1^\dagger \\ \text{---} \\ \text{---} \\ \text{---} \\ \phi_0 \quad \phi_1 \end{array} \quad (23)$$

where we have defined the state $|\hat{i}\rangle := H|i\rangle$, and $|i\rangle$ is the i th computational basis state. In Eq. (22) and Eq. (23), we have utilized the fact that

$$q \uparrow \begin{array}{c} \text{---} \\ \text{---} \\ \text{---} \\ \text{---} \\ \text{---} \end{array} = \begin{array}{c} \text{---} \\ \text{---} \\ \text{---} \\ \text{---} \\ \text{---} \end{array}, \quad HZH^\dagger = X \quad (24)$$

Thus we can write down the SICs as two explicit equations:

$$\begin{aligned} \langle R_x^\dagger(\vec{g}_0) Z^{-k} R_x(\vec{g}_0) \rangle_0 \langle X^k \rangle_1 &= 0, \\ \langle X^k \rangle_0 \langle R_x^\dagger(\vec{g}_1) Z^k R_x(\vec{g}_1) \rangle_1 &= 0 \end{aligned} \quad (25)$$

where $R_x(\vec{g}) := H^\dagger P(\vec{g})H$ and $k = 1, 2, \dots, q - 1$. For qubits, Eq. (25) will reduced to:

$$\begin{aligned} \langle R_x(g_0)^\dagger Z R_x(g_0) \rangle_0 \langle X \rangle_1 &= 0, \\ \langle X \rangle_0 \langle R_x(g_1)^\dagger Z R_x(g_1) \rangle_1 &= 0. \end{aligned} \quad (26)$$

That is, the product of the expectation value of Z rotated around the x -axis by g_0 and the expectation value of X is vanishing; and the product of the expectation value of X and the expectation value of Z rotated around the x -axis by g_1 is vanishing, respectively. There is a large family of product states that satisfy these. For example, when $g_0 = g_1 = 0$ (again for qubits), then the SICs reduce to

$$\begin{aligned} \langle Z \rangle_0 \langle X \rangle_1 &= 0, \\ \langle X \rangle_0 \langle Z \rangle_1 &= 0. \end{aligned} \quad (27)$$

The exhaustive set of solutions is the union of the sets $\{e^{-i\theta Z}|+\rangle \otimes e^{-i\theta' Z}|+\rangle\}, \{e^{-i\theta'' X}|0\rangle \otimes e^{-i\theta''' X}|0\rangle\}, \{|y, \pm\rangle \otimes |\psi\rangle\}, \{|\psi'\rangle \otimes |y, \pm\rangle\}$ where $\theta, \theta', \theta'', \theta'''$ are arbitrary angles and $|\psi\rangle, |\psi'\rangle$ are arbitrary qubit states. Here $|+\rangle = \frac{1}{\sqrt{2}}(|0\rangle + |1\rangle)$ and $|y, \pm\rangle = \frac{1}{\sqrt{2}}(|0\rangle \pm i|1\rangle)$.

IV. EARLY TIME ENTANGLEMENT DYNAMICS OF SIC STATES: EXACT LINEAR RAMP

We first present general analytic statements that can be made for early time entanglement dynamics. In particular, we claim that if the initial state of the subsystem A is prepared in a dimerized product state that satisfies the SIC, then $S(t) = 2t$ for $0 \leq t \leq N_A/4$ (we remind the reader $t \in \mathbb{N}$).

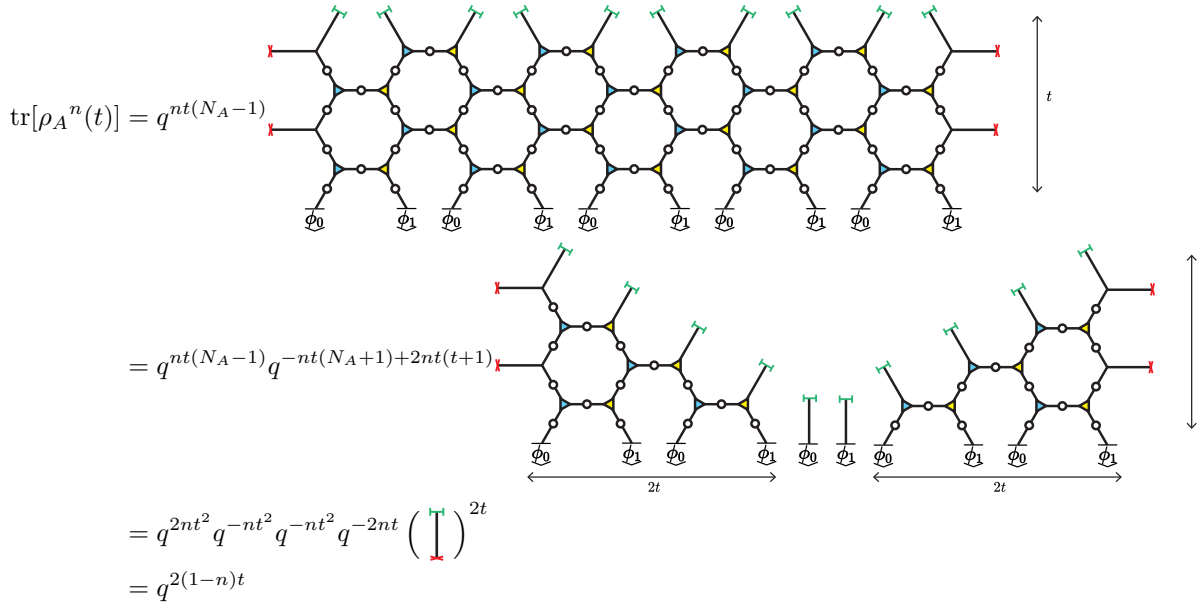
To prove this, we consider n replicas of the reduced density matrix ρ_A and calculate the generalized purities $\text{tr}[\rho_A^n(t)]$. Then, we take the limit $\lim_{n \rightarrow 1} S_n$, where S_n is the n -th Rényi entropy $S_n = \frac{1}{1-n} \log_q \text{tr}[\rho_A^n(t)]$. To avoid introducing excessive notation, in this section we temporarily generalize the meaning of bold tensors to denote n replicated pairs of forwards and backwards branches, for example



$$\quad (28)$$

(here depicted for $n = 3$). The third object represents the pairing of the n -th forward branch of the n pair with the $n - 1$ -th backward branch, used in the calculation of the generalized purity.

Then when $t \leq N_A/4$, using cancelation of the forwards and backwards branches, we have:



$$\begin{aligned} \text{tr}[\rho_A^n(t)] &= q^{nt(N_A-1)} \\ &= q^{nt(N_A-1)} q^{-nt(N_A+1)+2nt(t+1)} \\ &= q^{2nt^2} q^{-nt^2} q^{-nt^2} q^{-2nt} \left(\begin{array}{c} \text{---} \\ \text{---} \end{array} \right)^{2t} \\ &= q^{2(1-n)t} \end{aligned} \quad (29)$$

where in the first equality we use the unitary condition and in the second equality we use the SIC and triunitary/2DU conditions extensively, while in the third equality we use the following fact:

$$\begin{array}{c} \text{---} \\ | \\ \text{---} \end{array} = q. \quad (30)$$

Thus we have that $\text{tr}[\rho_A^n(t)] = q^{2(1-n)t}$, which implies that:

$$S(t) = \lim_{n \rightarrow 1} \frac{1}{1-n} \log_q \text{tr}[\rho_A^n(t)] = 2t, \quad (31)$$

i.e., there is no n -dependence of the n -th Rényi entropies $S_n = \frac{1}{1-n} \log_q \text{tr}[\rho_A^n(t)]$. From this calculation we note that we have also consequently derived that the entanglement spectrum of $\rho_A(t)$ (logarithm of the its eigenvalues) is flat (all eigenvalues are either zero or all non-zero but equal in value).

As a technical interlude, while the contraction of the tensor network proceeded straightforwardly enough, we see that the most tricky part of the calculation is keeping track of the coefficients (factors of q) that emerge upon simplification of different structures in the TN to factors of the basic diagram $\begin{array}{c} \text{---} \\ | \\ \text{---} \end{array}$.

We observe we can instead employ the following trick: we note all local rules of contraction hold true replacing green caps with red crosses, thus giving rise to the exact same coefficients during the intermediate steps. In the latter scenario however, we are calculating $\text{tr}[\rho_A(t)]^n$, which we know equals 1. Thus if we denote the coefficient of the final answer as $C(N_A, n, t)$, we have:

$$\text{tr}[\rho_A^n(t)] = C(N_A, n, t) \left(\begin{array}{c} \text{---} \\ | \\ \text{---} \end{array} \right)^{2t}, \quad \text{tr}[\rho_A(t)]^n = C(N_A, n, t) \left(\begin{array}{c} \text{---} \\ | \\ \text{---} \end{array} \right)^{2t} = C(N_A, n, t) q^{2nt} = 1. \quad (32)$$

This allows us to easily ascertain $C(N_A, n, t) = q^{-2nt}$. We will take this approach in the following sections regarding the replicated version of diagrams. In other words, this trick is nothing more than computing the tensor network of an unnormalized ρ_A , and then dividing by the normalization factor at the end of the day.

V. EXACT ENTANGLEMENT DYNAMICS OF THE AKIM WITH $\vec{g}_0 = \vec{0}$ AND ARBITRARY \vec{g}_1

Here, we concentrate on the dynamics for the AKIM $\vec{g}_0 = \vec{0}$ and generic \vec{g}_1 (recall by reflection symmetry all statements hold true upon swapping \vec{g}_0 with \vec{g}_1). The same analysis also applies for \vec{g}_0 having components which are π in value. Since we already demonstrated in the previous section all SIC states have exact linear ramps in their entanglement dynamics for early times $0 \leq t \leq N_A/4$, we concentrate on the times beyond this.

To begin, we note that when $\vec{g}_0 = \vec{0}$, the following local TN identities in the folded representation hold:

$$\begin{array}{c} \text{---} \\ | \\ \text{---} \end{array} \begin{array}{c} \text{---} \\ | \\ \text{---} \end{array} = \begin{array}{c} \text{---} \\ | \\ \text{---} \end{array} \begin{array}{c} \text{---} \\ | \\ \text{---} \end{array}, \quad \begin{array}{c} \text{---} \\ | \\ \text{---} \end{array} \begin{array}{c} \text{---} \\ | \\ \text{---} \end{array} = \frac{1}{q^2} \begin{array}{c} \text{---} \\ | \\ \text{---} \end{array}, \quad \begin{array}{c} \text{---} \\ | \\ \text{---} \end{array} = \frac{1}{q} \begin{array}{c} \text{---} \\ | \\ \text{---} \end{array} \quad (33)$$

When \vec{g}_0 has components containing π , e.g., for qubits $g_0 = \pi$, then identical looking diagrammatic identities hold:

$$\begin{array}{c} \text{---} \\ | \\ \text{---} \end{array} \begin{array}{c} \text{---} \\ | \\ \text{---} \end{array} = \begin{array}{c} \text{---} \\ | \\ \text{---} \end{array} \begin{array}{c} \text{---} \\ | \\ \text{---} \end{array}, \quad \begin{array}{c} \text{---} \\ | \\ \text{---} \end{array} \begin{array}{c} \text{---} \\ | \\ \text{---} \end{array} = \frac{1}{q^2} \begin{array}{c} \text{---} \\ | \\ \text{---} \end{array}. \quad (34)$$

We thus only consider the \vec{g}_0 case in what follows, for simplicity. Again, our strategy will be to compute the generalized purities $\text{tr}[\rho_A^n(t)]$ and take the limit of the Rényi entropies $S_n(t)$ as $n \rightarrow 1$. As before, we let bold tensors denote n -copy replicas of the basic tensors, as in Eq. (28).

A. Late time thermalization

We first establish that for *any* state, the system reaches the infinite temperature state when $t \geq N_A$ (“late-times”). This amounts to showing that the channel \mathcal{C} , when raised to the N_A -th power, becomes a rank-one projector onto

the identity operator. In other words, we desire to show $\mathcal{C}^{N_A} = q^{-N_A}|I\rangle\rangle\langle\langle I|$, where $|I\rangle\rangle$ is the vectorized identity operator. Utilizing Eq. (33) extensively, we compute:

$$\mathcal{C}^{N_A} \propto \dots \propto \dots \propto \dots \quad (35)$$

where we have utilized the triunitary/2DU properties to simplify the contractions from the third diagram onwards. Mathematically, this implies that \mathcal{C} has a Jordan block of at most N_A size.

Nevertheless, as stated in the main text, there is an entire family of dimerized initial states which can achieve earlier thermalization to the infinite-temperature state, which we call the “maximum-entanglement-solvable states”. Concretely, if we impose that the initial product state on A satisfies the SIC as well as the SEC, it will achieve $S(t) = N_A$ at $t \geq N_A/2$. The SEC additionally demands that the initial states $|\phi_0\rangle|\phi_1\rangle$ satisfy:

$$\dots = \dots \quad (36)$$

Let us understand what these solutions are. Writing the additional condition (36) out in unfolded TN, we have:

$$\dots = \dots \quad (37)$$

Solving (37) using the results from (24), we have:

$$\begin{array}{c} \widehat{\phi_0^\dagger} \\ \downarrow \\ \text{---} \text{---} \text{---} \text{---} \text{---} \\ \downarrow \\ \text{---} \text{---} \text{---} \text{---} \text{---} \\ \downarrow \\ \widehat{\phi_1^\dagger} \end{array} = 0, \quad i, j, k = 0, 1, \dots, q-1, j \neq k$$

$$\begin{array}{c} \widehat{\phi_0} \\ \downarrow \\ \text{---} \text{---} \text{---} \text{---} \text{---} \\ \downarrow \\ \text{---} \text{---} \text{---} \text{---} \text{---} \\ \downarrow \\ \widehat{\phi_1} \end{array}$$
(38)

Writing it out explicitly, we have:

$$\langle \phi_0 | -i - k \rangle \langle -i - j | \phi_0 \rangle \langle \phi_1 | H^\dagger | k \rangle \langle j | H | \phi_1 \rangle = 0 \quad (39)$$

where $|-i - k\rangle := |-i - k \pmod{q}\rangle$. For qubit case, (39) will reduced to:

$$\langle \phi_0 | 0 \rangle \langle 1 | \phi_0 \rangle \langle \phi_1 | H^\dagger | 0 \rangle \langle 1 | H | \phi_1 \rangle = 0 \quad (40)$$

Here, we define:

$$|z^\perp; \vec{h}\rangle := P(\vec{h})H|0\rangle \quad (41)$$

$$|x^\perp; \vec{h}\rangle := HP(\vec{h})H|0\rangle \quad (42)$$

From construction, we know that $\langle z^\perp; \vec{h} | Z | z^\perp; \vec{h} \rangle = 0$ and $\langle x^\perp; \vec{h} | X | x^\perp; \vec{h} \rangle = 0$. For simplicity of expression, when \vec{h} is not specified, we denote $|z^\perp; \vec{h}\rangle$ and $|x^\perp; \vec{h}\rangle$ as $|z^\perp\rangle$ and $|x^\perp\rangle$. For qubit case, we can prove that the exhaustive set of $|\phi_0\rangle \otimes |\phi_1\rangle$ satisfying the SEC is $\{|z\rangle \otimes |x^\perp\rangle\} \cup \{|z^\perp\rangle \otimes |x\rangle\}$. For qudit in generic dimension, we can verify the set $\{|z\rangle \otimes |x^\perp\rangle\} \cup \{|z^\perp\rangle \otimes |x\rangle\}$ satisfies the SEC, where $|x\rangle := H|z\rangle$.

For this class of states, we then have:

$$\begin{array}{l} \rho_A(t = N_A/2) \propto \end{array}$$

$$\begin{array}{l} \propto \\ \propto \\ \propto \end{array}$$
(43)

as claimed. In going from the second to the third diagram, we ‘opened’ up the diagram starting from the bottom right owing to unitarity in the north-west direction.

B. Thermalizing dynamics of maximum-entanglement-solvable states for intermediate times

Now we show that the maximum-entanglement-solvable states's full dynamics can be analytically computed for *all* times. Since we have already shown this for early-times $0 \leq t \leq N_A/4$ and late times $t \geq N_A$, we focus on the intermediate times $N_A/4 < t < N_A$.

The generalized purity is given by:

$$\begin{aligned}
 \text{tr}[\rho_A^n(t)] &\propto \text{Diagram 1} \propto \text{Diagram 2} \\
 &= \text{Diagram 3} = \text{Diagram 4} \\
 &\propto \text{Diagram 5}
 \end{aligned} \tag{44}$$

Going from the first diagram to the fourth utilizes Eq. (33). In particular, in going from the second to the third, we have added red crosses to the states and also removed a red cross on the top left. From the third to fourth diagram we have removed all red crosses in the bulk, which allows us to cancel many of the gates due to unitarity.

Now since

$$\begin{aligned}
 \text{---} \times |z\rangle &= \text{---} |z\rangle, & \text{---} \times |z^\perp; \bar{h}\rangle &= q^{-n} \text{---}
 \end{aligned} \tag{45}$$

we can verify that the set of maximum-entanglement-solvable states $\{|z\rangle \otimes |x^\perp\rangle\} \cup \{|z^\perp\rangle \otimes |x\rangle\}$ satisfies:

$$\begin{aligned}
 \text{Diagram 6} &= q^{-3n} \text{Diagram 7},
 \end{aligned} \tag{46}$$

allowing us to contract the TN further so that the generalized purity ultimately takes the form:

$$\text{tr}[\rho_A^n(t)] \propto \text{Diagram 8} \propto \left(\begin{array}{c} \text{---} \\ \text{---} \\ \text{---} \\ \text{---} \end{array} \right)_{\phi_0, \phi_1}^{N_A/2-t} \left(\begin{array}{c} \text{---} \\ \text{---} \\ \text{---} \\ \text{---} \end{array} \right)^{4t-N_A+N_A/2-t} \tag{47}$$

Again, for the maximum-entanglement-solvable states, $\{|z\rangle \otimes |x^\perp\rangle\} \cup \{|z^\perp\rangle \otimes |x\rangle\}$, we can verify that

$$\begin{array}{c} \begin{array}{|c|} \hline \color{red}{\mathbb{I}} \\ \hline \color{red}{\otimes} \\ \hline \color{red}{\mathbb{I}} \\ \hline \end{array} \\ \color{red}{\otimes} \\ \begin{array}{|c|} \hline \color{red}{\mathbb{I}} \\ \hline \color{red}{\otimes} \\ \hline \color{red}{\mathbb{I}} \\ \hline \end{array} \end{array} = q^{-n} \begin{array}{|c|} \hline \color{red}{\mathbb{I}} \\ \hline \color{red}{\otimes} \\ \hline \color{red}{\mathbb{I}} \\ \hline \end{array} \quad (48)$$

which finally allows us to declare

$$\text{tr}[\rho_A^n(t)] \propto \left(\begin{array}{|c|} \hline \color{red}{\mathbb{I}} \\ \hline \color{red}{\otimes} \\ \hline \color{red}{\mathbb{I}} \\ \hline \end{array} \right)^{2t} \quad (49)$$

From the argument at the end of Sec. IV regarding the appropriate normalization, we thus have that $\text{tr}[\rho_A^n(t)] = q^{2(1-n)t}$ and

$$S(t) = \lim_{n \rightarrow 1} \frac{1}{1-n} \log_q \text{tr}[\rho_A^n(t)] = \lim_{n \rightarrow 1} \frac{1}{1-n} \log_q q^{2(1-n)t} = 2t \quad (50)$$

VI. ENTANGLEMENT DYNAMICS OF AKIM AT $(g_0, g_1) = ((2n+1)\pi/2, (2m+1)\pi/2)$

In this section, we focus on qubit systems, and on the AKIM at parameters $g_0 = (2n+1)\pi/2, g_1 = (2m+1)\pi/2$ where $n, m \in \mathbb{Z}$, as was considered in the main text. We note all analyses can be extended to the case of qudits with necessary changes.

We first make a preliminary analysis reducing all analyses down to the single case of $g_0 = \pi/2, g_1 = \pi/2$. First, dynamics of the AKIM at these parameter points are all Clifford [4]. This implies that the circuit U^t at one set of parameters is equal to another, up to some string of Pauli operators. Second, it can be easily verified the dimerized states fulfilling SICs are identical for all parameters $g_0 = (2n+1)\pi/2, g_1 = (2m+1)\pi/2$. Combined, this means that the channels \mathcal{C} governing local dynamics on A are also related to one another by the action of only an additional Pauli channel. Immediately this implies entanglement dynamics of the AKIM is identical in this family of parameters (as long as we prepare the same state), and so we can focus on the case $(g_0, g_1) = (\pi/2, \pi/2)$.

However, if we are interested in the reduced density matrices themselves, we have to understand the channels themselves. It is straightforward to work out the following relations between them. Let $\mathcal{C}_{1(3)/2, 1(3)/2}$ denote the channel of the AKIM at the parameters $(g_0, g_1) = (1(3) \times \pi/2, 1(3) \times \pi/2)$. Then we can easily check that:

$$\begin{aligned} \mathcal{P}_{IYIY\dots} \circ \mathcal{C}_{1/2, 1/2}^t &= \mathcal{C}_{1/2, 3/2}^t \text{ for } t = 4n + 1, n \in \mathbb{N} \\ \mathcal{P}_{YYYY\dots} \circ \mathcal{C}_{1/2, 1/2}^t &= \mathcal{C}_{1/2, 3/2}^t \text{ for } t = 4n + 2, n \in \mathbb{N} \\ \mathcal{P}_{YIYI\dots} \circ \mathcal{C}_{1/2, 1/2}^t &= \mathcal{C}_{1/2, 3/2}^t \text{ for } t = 4n + 3, n \in \mathbb{N} \\ \mathcal{C}_{1/2, 1/2}^t &= \mathcal{C}_{1/2, 3/2}^t \text{ for } t = 4n + 4, n \in \mathbb{N}, \end{aligned} \quad (51)$$

where $\mathcal{P}_P[\rho] = \frac{1}{2}(\rho + P\rho P^\dagger)$ for a Pauli string P ; and

$$\begin{aligned} \mathcal{P}_{YYYY\dots} \circ \mathcal{C}_{1/2, 1/2}^t &= \mathcal{C}_{3/2, 3/2}^t \text{ for } t = 2n + 1, n \in \mathbb{N} \\ \mathcal{C}_{1/2, 1/2}^t &= \mathcal{C}_{3/2, 3/2}^t \text{ for } t = 2n + 2, n \in \mathbb{N}. \end{aligned} \quad (52)$$

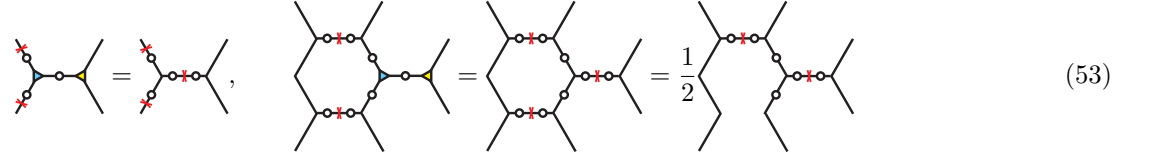
This will allow us to focus on only the case of $(g_0, g_1) = (\pi/2, \pi/2)$, whereupon we can translate all results from there to other cases, with consideration of the action of the additional Pauli channel.

Let us state a summary of our findings:

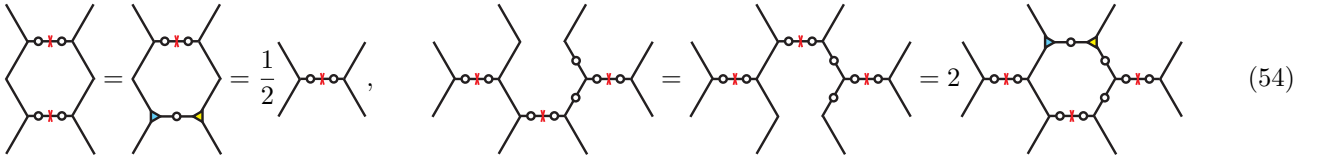
- As argued above, entanglement dynamics of a given state is the same for any parameter values of the AKIM of the form $((2n+1)\pi/2, (2m+1)\pi/2)$.
- For $(g_0, g_1) = (\pi/2, \pi/2)$, $\mathcal{C}_{1/2, 1/2}^{N_A/2+1} = \mathcal{C}_{1/2, 1/2}^{N_A/2+2}$. This implies the system always equilibrates regardless of initial state at time $t = N_A/2 + 1$.
- However, there are multiple steady states — the equilibrium state is not unique. This is because of the existence of an exponential (i.e., super-extensive!) set of conserved quantities: 2^{N_A-1} operators consisting of independent products of $Z_i Z_{i+1}$ on odd bonds and $X_i X_{i+1}$ on even bonds.

- For $(g_0, g_1) = (3\pi/2, 3\pi/2)$, we also have $\mathcal{C}_{3/2,3/2}^{N_A/2+1} = \mathcal{C}_{3/2,3/2}^{N_A/2+2}$, i.e., equilibration regardless of initial state at $t = N_A/2 + 1$. This is because the channel $\mathcal{P}_{Y\bar{Y}Y\bar{Y}\dots}$ acts trivially on the conserved quantities of $(g_0, g_1) = (\pi/2, \pi/2)$, so that $\mathcal{C}_{3/2,3/2}^t = \mathcal{C}_{1/2,1/2}^t$ for $t \geq N_A/2 + 1$.
- For $(g_0, g_1) = (\pi/2, 3\pi/2)$ the situation is more interesting. It can be seen $\mathcal{P}_{I\bar{Y}I\bar{Y}\dots}$ has the same action as $\mathcal{P}_{Y\bar{Y}Y\bar{Y}\dots}$ on the conserved quantities which is non-trivial (some operators pick up under a minus sign under this channel, for example $Z_1 Z_2$). Thus, for $t \geq N_A/2 + 1$, we have $\mathcal{C}_{1/2,3/2}^t = \mathcal{P}_{I\bar{Y}I\bar{Y}} \circ \mathcal{C}_{1/2,1/2}^t$ for $t = 2n + 1, n \in \mathbb{N}$ and $\mathcal{C}_{1/2,3/2}^t = \mathcal{C}_{1/2,1/2}^t$ for $t = 2n + 2, n \in \mathbb{N}$, i.e., the system oscillates between two ‘steady’-states.

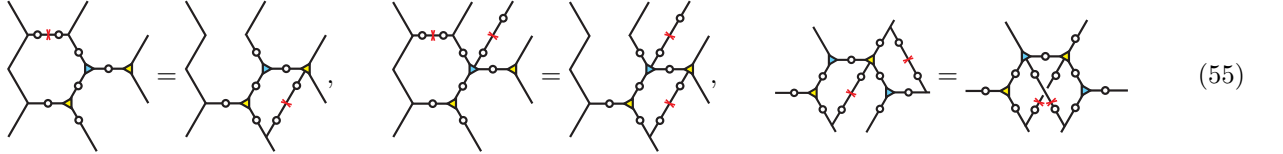
Let us now prove these statements. When $g_0 = g_1 = \frac{\pi}{2}$, we identify the following local TN contraction rules:



$$(53)$$



$$(54)$$



$$(55)$$

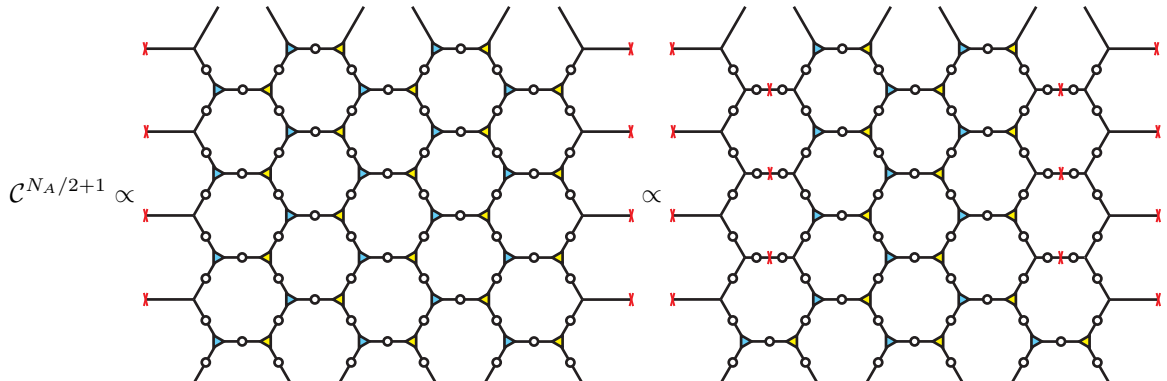
Note in the last figure, there is an avoided crossing of lines. We will use Eqs. (53) and (54) extensively in the following calculation for finite-time entanglement saturation, where Eq. (53) serves as the rule describing the emergence of red cross tensors in the bulk of the subsystem, and Eq. (54) is the useful diagrammatic tool for reduction of the TN. We will use Eq. (55) in the computation of entanglement dynamics.

A. Exact finite time entanglement saturation

We claim that the quantum channel \mathcal{C} for subsystem A has the following property:

$$\mathcal{C}^{N_A/2+k} = \mathcal{C}^{N_A/2+1}, \quad \forall k \in \mathbb{N}^+. \quad (56)$$

To prove this property we first derive the diagrammatic expression for $\mathcal{C}^{N_A/2+1}$:



$$\propto \quad \propto \quad (57)$$

where we have used the previously quoted local TN identities and also used the first equation of Eq. (33). Since unitality enforces $\mathcal{C}^{N_A/2+1}[I] = I$, this fixes the normalization constant:

$$\mathcal{C}^{N_A/2+1} = 2^{N_A-1} \quad \propto \quad (58)$$

Next we prove that $\mathcal{C}^{N_A/2+2} = \mathcal{C}^{N_A/2+1}$. We notice:

$$\mathcal{C}^{N_A/2+2} \propto \quad \propto \quad \mathcal{C}^{N_A/2+1} \quad (59)$$

By unitality this fixes the normalization constant again so that $\mathcal{C}^{N_A/2+2} = \mathcal{C}^{N_A/2+1}$ and we can then complete the proof of Eq. (56) by induction.

It is instructive to understand physically the action of the late-time channel $\mathcal{C}^{N_A/2+1}$. From the folded TN representation of $\mathcal{C}^{N_A/2+1}$, we notice that it is a composition of three local channels:

$$c = 2 \quad , \quad c[\rho] = \frac{1}{2}(\rho + (X \otimes X)\rho(X \otimes X)) \quad (60)$$

$$d = 2 \quad , \quad d[\rho] = \frac{1}{2}(\rho + (Z \otimes Z)\rho(Z \otimes Z)) \quad (61)$$

$$b = 1 \quad , \quad b[\rho] = \frac{1}{2}(\rho + Z\rho Z) \quad (62)$$

Then we have:

$$\mathcal{C}^{N_A/2+1} = b_1 \circ b_{N_A} \circ \prod_{\text{even bonds}} d \circ \prod_{\text{odd bonds}} c \quad (63)$$

In other words, the late-time channel describes XX dissipation on odd bonds followed by ZZ dissipation on even bonds, and lastly Z -dephasing on the boundaries.

We can fully understand the spectral decomposition of the late-time channel $\mathcal{C}^{N_A/2+1}$. Since it is the composition of local channels which are all Pauli channels, its eigenvectors are all Pauli strings, and its eigenvalues are 1 or 0. Precisely, the set of Pauli strings that commutes with all of the Kraus operators of the local channels are the eigenvectors with unity eigenvalues, and are hence conserved quantities in dynamics, while the set of Pauli strings which commutes with at least one Kraus operator are the eigenvectors with zero eigenvalues. The former set is exhausted by all independent products of ZZ operators on odd bonds and XX operators on even bonds, of which there are 2^{N_A-1} of them. For example, for $N_A = 4$, we have 8 operators $IIII, ZZII, IIZZ, IXXI, ZYXI, IXYZ, ZYYZ, ZZZZ$.

B. Exact entanglement dynamics with maximal saturation of entropy

Although there are super-extensive conserved quantities for the case of $g_0 = g_1 = \pi/2$, we can still achieve thermalization to infinite temperature with exact linear growth of entanglement for some specific states. Here we prove that for the large family of dimerized product states $|z\rangle \otimes |z^\perp\rangle$ and $|y\rangle \otimes |x^\perp\rangle$, they have linear entanglement growth with slope 2 and reach the infinite-temperature state when $t \geq N_A/2$. In other words,

$$S(t) = \min(2t, N_A). \quad (64)$$

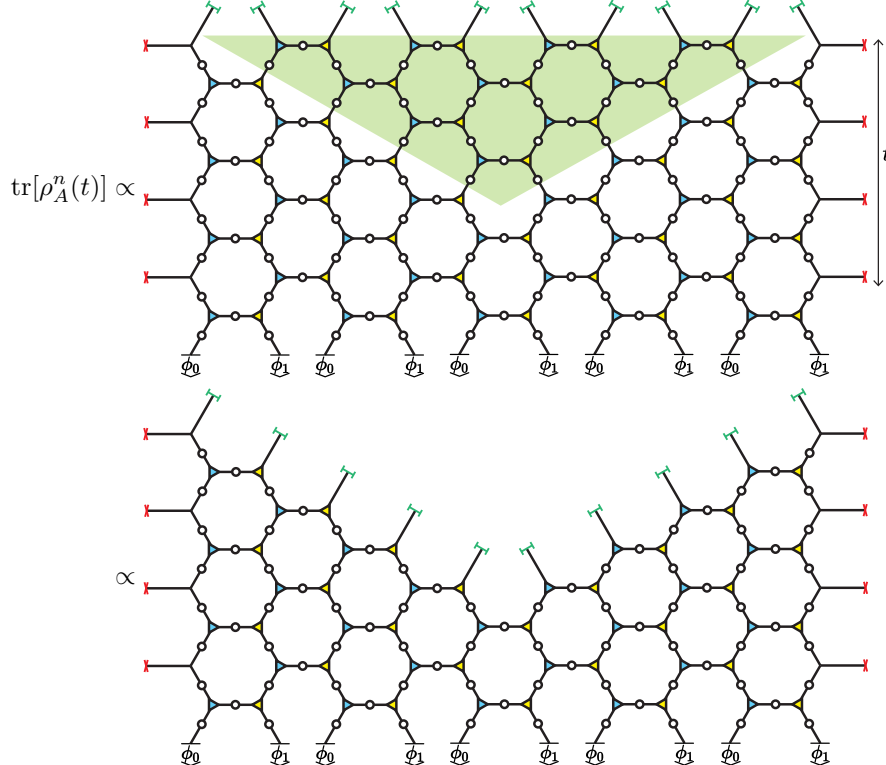
Note that by symmetry, this holds true for $|z^\perp\rangle \otimes |z\rangle$ and $|y^\perp\rangle \otimes |x\rangle$ too. We dub these the “maximum-entanglement-solvable” states.

We take the following approach. First, we will prove that for $t \leq N_A/2$, we have $\text{tr}[\rho_A^n(t)] = 2^{2t(1-n)}$ and thus $S(t) = 2t$. This then implies $\rho_A(N_A/2) \propto I_A$ as it is the unique state with maximal entropy, which is then seen to be a steady-state for times $t \geq N_A/2$. For the calculation, we will use the following fact extensively:

$$\begin{array}{c} \text{---} \text{---} \text{---} \\ | \\ \text{---} \end{array} = \frac{1}{q} \text{---} \text{---} \quad (65)$$

to break up the TN diagram. We note an analogous relation holds upon changing a green end into a red cross (they just represent different pairings of forwards and backwards branches of the n replicas).

To begin, we observe $|z\rangle \otimes |z^\perp\rangle$ and $|y\rangle \otimes |x^\perp\rangle$ satisfy the SIC, so they achieve exact linear entanglement growth for $t \leq N_A/4$ as we proved in Sec. IV. For intermediate times $N_A/4 \leq t \leq N_A/2$ we have the following diagram, which we can contract:



$$\begin{aligned}
& \propto \\
& = \\
& = \\
& \propto \langle L_1 | \quad T_l \quad T_m \quad T_r \quad | R_1 \rangle \\
& = \langle L_1 | T_l^{N_A/2-t} T_m^{2t-N_A/2-1} T_r^{N_A/2-t} | R_1 \rangle
\end{aligned} \tag{66}$$

Above, l stands for left; m for middle; and r for right. Going from the first line to the second, we canceled gates within the causal light-cone away from the boundaries (green triangle); from the second to third, we used Eqs. (53) and (54); in moving to the fourth, fifth and sixth line we used (55) repeatedly.

The end result, Eq. (66), is an elucidation of the general, simplified structure of the generalized purity in the intermediate time regime: it is a 1D diagram consisting of contraction of boundary states $\langle L_1, |R_1\rangle$ within bulk tensors T_l, T_m, T_r of varying numbers depending on system size N_A and time t .

Now we contract the 1D TN, Eq. (66), for the states $|\phi_0\rangle \otimes |\phi_1\rangle = |z\rangle \otimes |z^\perp\rangle$. We have

$$\langle L_1 | T_l = \text{[Diagram]} = \text{[Diagram]} \propto \text{[Diagram]} \tag{67}$$

$$\propto \text{[Diagram 1]} \propto \text{[Diagram 2]} \quad (68)$$

where for the second equality, we used the results from the first equalities of Eq. (45) and Eq. (53); and for the first proportionality we used the two equalities of Eq. (45) since $H|z\rangle \in \{|z^\perp\rangle\}$. Next define

$$\langle L_2| := \text{[Diagram 3]} \quad (69)$$

We will see this same structure is preserved as we perform contraction of the 1D TN Eq. (66) going from left to right, with factors $\begin{array}{|c} \hline \hline \end{array}$ ‘popping’ out.

Indeed, applying $\langle L_2|$ with T_l we have

$$\langle L_2|T_l = \text{[Diagram 4]} \propto \text{[Diagram 5]} \propto \text{[Diagram 6]} \propto \text{[Diagram 7]} = \begin{array}{|c} \hline \hline \end{array} \langle L_2|, \quad (70)$$

while for T_m ,

$$\langle L_2|T_m = \text{[Diagram 8]} \propto \text{[Diagram 9]} \propto \text{[Diagram 10]} \propto \text{[Diagram 11]} \propto \begin{pmatrix} \hline \hline \end{pmatrix}^2 \langle L_2|. \quad (71)$$

For T_r ,

$$\langle L_2|T_r = \text{[Diagram 12]} \propto \text{[Diagram 13]} \propto \text{[Diagram 14]} \propto \text{[Diagram 15]} = \begin{array}{|c} \hline \hline \end{array} \langle L_2|. \quad (72)$$

Lastly, we take the overlap of $\langle L_2|$ with the right boundary state $|R_1\rangle$.

$$\langle L_2|R_1 = \text{[Diagram 16]} \propto \text{[Diagram 17]} \propto \begin{array}{|c} \hline \hline \end{array} = \begin{array}{|c} \hline \hline \end{array} \quad (73)$$

So if $N_A/2 \leq t < N_A/2$, we can see $\text{tr}[\rho_A^n(t)] \propto \left(\begin{array}{|c} \hline \hline \end{array}\right)^{2t}$. For the special case of $t = N_A/2$, we instead have:

$$\text{tr}[\rho_A^n(N_A/2)] = \langle L_1|T_m^{N_A/2-1}|R_1\rangle. \quad (74)$$

Now since

$$\langle L_1|T_m = \text{[Diagram 18]} \propto \text{[Diagram 19]} \propto \text{[Diagram 20]} \quad (75)$$

$$= \text{[Diagram 21]} \propto \text{[Diagram 22]} \propto \text{[Diagram 23]} = \begin{pmatrix} \hline \hline \end{pmatrix}^2 \langle L_1|, \quad (76)$$

and

$$\langle L_1|R_1 = \text{[Diagram 24]} = \text{[Diagram 25]} \propto \text{[Diagram 26]} \propto \begin{pmatrix} \hline \hline \end{pmatrix}^2, \quad (77)$$

therefore

$$\text{tr}[\rho_A^n(N_A/2)] \propto \left(\prod_{\perp} \right)^{N_A} \implies \text{tr}[\rho_A^n(N_A/2)] = 2^{N_A(1-n)}. \quad (78)$$

Conversely for $|\phi_0\rangle \otimes |\phi_1\rangle = |y\rangle \otimes |x^\perp\rangle$, we notice that

$$\langle L_1 | T_l = \text{Diagram 1} = \text{Diagram 2} = \text{Diagram 3} \propto \text{Diagram 4} \propto \text{Diagram 5} \quad (79)$$

$$\langle L_1 | T_m = \text{Diagram 6} = \text{Diagram 7} \propto \text{Diagram 8} \quad (80)$$

$$\propto \text{Diagram 9} \propto \text{Diagram 10} \propto \text{Diagram 11} \quad (81)$$

$$\text{Tr} |R_1\rangle = \text{Diagram 12} \propto \text{Diagram 13} \propto \text{Diagram 14} \propto \text{Diagram 15} \propto |R_1\rangle \quad (82)$$

$$\langle L_1 | R_1\rangle = \text{Diagram 16} = \text{Diagram 17} \propto \text{Diagram 18} \propto \left(\prod_{\perp} \right)^2 \quad (83)$$

Thus for $t \leq N_A/2$, $\text{tr}[\rho_A^n(t)] \propto \left(\prod_{\perp} \right)^{2t}$ in both scenarios, which implies $\text{tr}[\rho_A^n(t)] = 2^{2t(1-n)}$ and hence $S_n(t) = 2t$. Upon taking the analytic continuation $n \rightarrow 1$ of the n -th Rényi entropies we thus obtain our claimed result for the von Neumann entropy $S(t)$.

C. Exact entanglement dynamics with non-maximal saturation of entropy

Here we demonstrate a state for which exact entanglement dynamics can be computed, though saturation of entropy is non-maximal. Specifically we prove that for $|\phi_0\rangle \otimes |\phi_1\rangle = |z\rangle \otimes |z\rangle$, we have

$$S(t) = \min\{2t, N_A/2\}. \quad (84)$$

(Recall $t \in \mathbb{N}$).

We first notice that $|z\rangle \otimes |z\rangle$ satisfies the SIC condition, which means that we already have exact linear growth of entanglement dynamics when $t \leq N_A/4$, with slope 2. For $t \geq N_A/2 + 1$, we have:

$$\begin{aligned} \text{tr}[\rho_A^n(t)] &\propto \text{Diagram 19} \propto \text{Diagram 20} \\ &\propto \text{Diagram 21} \propto \text{Diagram 22} \\ &\propto \text{Diagram 23} = \left(\prod_{\perp} \right)^{N_A/2} \end{aligned} \quad (85)$$

Then we focus on the regime $N_A/4 < t \leq N_A/2$. We have

$$\mathrm{tr}[\rho_A^n(t)] \propto \langle L_1 | T_l^{N_A/2-t} T_m^{2t-N_A/2-1} T_r^{N_A/2-t} | R_1 \rangle, \quad (86)$$

as stated in the former subsection. Since

$$\langle L_1 | T_l = \begin{array}{c} \text{Diagram 1} \\ \text{Diagram 2} \end{array} \propto \begin{array}{c} \text{Diagram 3} \\ \text{Diagram 4} \end{array} \propto \begin{array}{c} \text{Diagram 5} \\ \text{Diagram 6} \end{array} \propto \begin{array}{c} \text{Diagram 7} \\ \text{Diagram 8} \end{array} \propto \langle L_1 | \quad (87)$$

$$\langle L_1 | T_m = \begin{array}{c} \text{Diagram 9} \\ \text{Diagram 10} \end{array} \propto \begin{array}{c} \text{Diagram 11} \\ \text{Diagram 12} \end{array} \propto \begin{array}{c} \text{Diagram 13} \\ \text{Diagram 14} \end{array} \propto \langle L_1 | \quad (88)$$

Analogous to the calculation for $\langle L_1 | T_l$, undergoing contraction from right to left instead of from left to right, we find:

$$T_r | R_1 \rangle = \begin{array}{c} \text{Diagram 15} \\ \text{Diagram 16} \end{array} \propto \begin{array}{c} \text{Diagram 17} \\ \text{Diagram 18} \end{array} | R_1 \rangle. \quad (89)$$

Additionally, we have:

$$\langle L_1 | R_1 \rangle = \begin{array}{c} \text{Diagram 19} \\ \text{Diagram 20} \end{array} = \begin{array}{c} \text{Diagram 21} \\ \text{Diagram 22} \end{array} \propto \begin{array}{c} \text{Diagram 23} \\ \text{Diagram 24} \end{array} \propto \begin{array}{c} \text{Diagram 25} \\ \text{Diagram 26} \end{array}. \quad (90)$$

Thus for $N_A/4 < t \leq N_A/2$, we obtain $\mathrm{tr}[\rho_A^n(t)] \propto \left(\begin{array}{c} \text{Diagram 27} \\ \text{Diagram 28} \end{array} \right)^{N_A/2}$, leading to the fact that $\mathrm{tr}[\rho_A^n(t)] = 2^{(1-n)N_A/2}$, and upon performing an analytic continuation $n \rightarrow 1$ our stated claim of $S(t)$.

VII. GAP OF QUANTUM CHANNEL \mathcal{C}

In this section, we numerically investigate the channel \mathcal{C} governing dynamics on A , Eq. (21). In particular, we compute the gap Δ defined as

$$\Delta := 1 - \max_{\lambda: |\lambda| < 1} |\lambda| \quad (91)$$

where λ is the eigenvalue of \mathcal{C} not belonging to the eigenvector which is the identity operator, which physically sets the rate of thermalization. This is shown in Fig. 1 for $N_A = 4$.

We see from Fig. 1 that along $g_0 = 0, \pi$ or $g_1 = 0, \pi$, $\Delta = 1$, indicating that the maximally-mixed state \mathbb{I} is the unique unity eigenvector, and all other eigenvectors carry zero eigenvalues. This implies that thermalization to infinite-temperature is necessarily attained at some finite time. At $g_0 = g_1 = \pi/2$, $g_0 = \pi/2, g_1 = 3\pi/2$, $g_0 = 3\pi/2, g_1 = \pi/2$, and $g_0 = g_1 = 3\pi/2$, we see $\Delta = 0$, indicating the presence of degenerate steady-states or oscillatory non-decaying states. Finally, for generic g_0, g_1 away from these special regions, we see $0 < \Delta < 1$, indicating the system has a unique steady-state (the identity operator), and that the approach only is generically attained exponentially quickly (as opposed to exactly at some finite time), with the rate set by the gap Δ .

VIII. TRACKING STABILIZERS AND OPERATOR ENTANGLEMENT

We consider the AKIM on a system of qubits in this section. For the ‘‘maximum-entanglement-solvable’’ states found for g_0 (or for $g_1 = g_2 = \pi/2$), our calculation in Sec. V (and Sec. VI) yielded that the n -th Rényi entropy of the

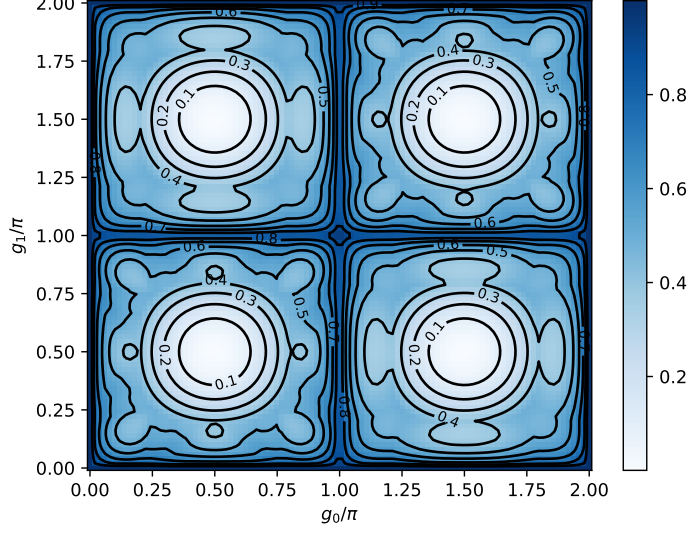


FIG. 1. Gap Δ of the channel \mathcal{C} at different parameters (g_0, g_1) of the AKIM. We see the gap is 1 along the lines $g_0 = 0, \pi$ and $g_1 = 0, \pi$, while it is 0 at $g_0 = (2n+1)\pi/2, g_1 = (2m+1)\pi/2$, where $n, m \in \mathbb{Z}$.

RDM $\rho_A(t)$ is $\min(2t, N_A)$ and in particular independent of n , indicating that its entanglement spectrum (logarithm of eigenvalues of $\rho_A(t)$) is flat at any time. Thus, we *must* be able to decompose $\rho_A(t)$ into products of projectors

$$\rho_A(t) = \frac{1}{2^{N_A}} \prod_{n=1}^{N_A - \min(2t, N_A)} (1 + O_n^{(t)}) \quad (92)$$

where $O_n^{(t)}$ are Hermitian operators satisfying $[O_n^{(t)}, O_m^{(t)}] = 0$ and $\text{eig}(O_n^{(t)}) = \pm 1$ with equal degeneracies. In other words, $O_n^{(t)}$ are the *stabilizers* of the RDM at a given time t . Of course, we note that this decomposition is not unique, as products of stabilizers yield new valid stabilizers; one just has to pick a maximal set of algebraically independent ones.

Our aim here is to investigate the fine-structure of these stabilizers; in particular, their operator entanglement. Concretely, we fix $N_A = 6$, $g_0 = 0$, allow arbitrary g_1 , and consider the initial state on A prepared as a dimerized product state $|0\rangle \otimes e^{i\theta X} |0\rangle$.

At time $t = 0$, since $\rho_A(t)$ is a product state, it is easy to write down its stabilizers:

$$\begin{aligned} O_1^{(1)} &= Z_1, \\ O_2^{(1)} &= \cos(2\theta)Z_2 + \sin(2\theta)Y_2, \\ O_3^{(1)} &= Z_3, \\ O_4^{(1)} &= \cos(2\theta)Z_4 + \sin(2\theta)Y_4, \\ O_5^{(1)} &= Z_5, \\ O_6^{(1)} &= \cos(2\theta)Z_6 + \sin(2\theta)Y_6. \end{aligned} \quad (93)$$

At $t = 1$, we find

$$\begin{aligned} O_1^{(2)} &= Z_1 X_2 \\ O_2^{(2)} &= Z_3 X_4 \\ O_3^{(2)} &= (\cos(g_1 + 2\theta)X_3 - \sin(g_1 + 2\theta)Y_3)Z_4 \\ O_4^{(2)} &= (\cos(g_1 + 2\theta)X_5 - \sin(g_1 + 2\theta)Y_5)Z_6 \end{aligned} \quad (94)$$

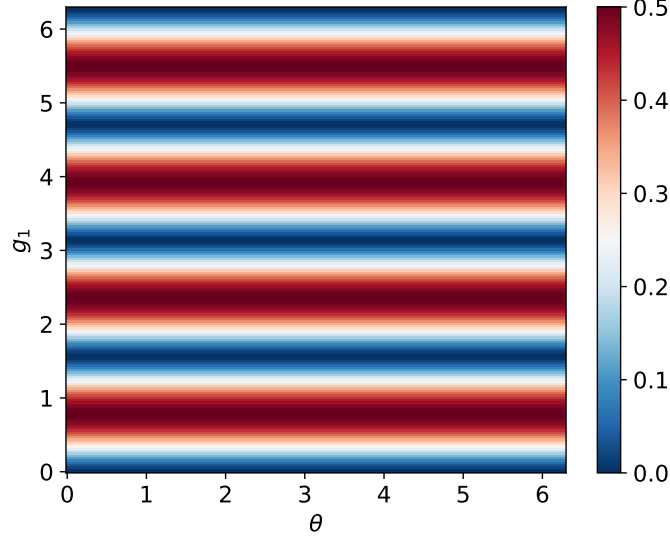


FIG. 2. Operator entanglement entropy of stabilizer $O^{(2)}$. Away from the Clifford points $g_1 = n\pi/2$, the stabilizer develops a complicated spatial structure, captured by the presence of operator entanglement.

While more complicated than the stabilizers at $t = 0$ (they are now more non-local), they are all still expressible as a tensor product of local operators $o_i \otimes o_j$ on sites i, j , i.e., they do not harbor operator entanglement.

The situation is more interesting when $t = 2$. We find

$$\begin{aligned}
O_1^{(2)} &= Z_1 Z_3 X_4, \\
O_2^{(2)} &= s_{g_1} c_{g_1} c_{2(g_1+\theta)} X_3 Y_4 Z_6 - s_{g_1} s_{g_1} s_{2(g_1+\theta)} X_3 Y_4 Z_5 Z_6 + c_{g_1} c_{g_1} c_{2(g_1+\theta)} X_3 Z_4 Z_6 - s_{g_1} c_{g_1} s_{2(g_1+\theta)} X_3 Z_4 Z_5 Z_6 \\
&\quad - s_{g_1} c_{g_1} s_{2(g_1+\theta)} Y_3 Y_4 Z_6 - s_{g_1} s_{g_1} c_{2(g_1+\theta)} Y_3 Y_4 Z_5 Z_6 - c_{g_1} c_{g_1} s_{2(g_1+\theta)} Y_3 Z_4 Z_6 - s_{g_1} c_{g_1} c_{2(g_1+\theta)} Y_3 Z_4 Z_5 Z_6, \quad (95)
\end{aligned}$$

where $c_x = \cos(x)$ and $s_x = \sin(x)$. While $O_1^{(2)}$ is simple, $O_2^{(2)}$ appears complicated (furthermore, this complexity is preserved even if we consider their product, $O_1^{(2)} O_2^{(2)}$).

We probe $O_2^{(2)}$'s operator entanglement entropy for a bipartition into sites 1 : 3 (L), and sites 4 : 6 (R). This is defined as follows. We write $O_2^{(2)}$ in its Schmidt decomposition

$$O_2^{(2)} = \sum_i \sqrt{p_i} O_{i,L} \otimes O_{i,R} \quad (96)$$

where $O_{i,L}, O_{j,L}$ are assumed to be mutually orthonormal under the Hilbert-Schmidt inner product, $O_{i,R}, O_{j,R}$ are assumed to be mutually orthonormal under the Hilbert-Schmidt inner product, and $p_i \geq 0$. The operator entanglement is defined to be the Shannon entropy associated with $\{p_i\}$. A simpler and alternative way to understand it is to treat the operators as living in a vector space, so that we can formally map $I \mapsto |0\rangle$, $X \mapsto |1\rangle$, $Y \mapsto |2\rangle$, $Z \mapsto |3\rangle$ and consider the entanglement entropy of the resulting quantum state. Since $O_2^{(2)}$ has no support on sites 1, 2 and since it has a common action Z_6 on site 6, the operator entanglement entropy reduces to the bipartite entanglement entropy of the state

$$\begin{aligned}
|\psi\rangle &= s_{g_1} c_{g_1} c_{2(g_1+\theta)} |120\rangle - s_{g_1} s_{g_1} s_{2(g_1+\theta)} |123\rangle + c_{g_1} c_{g_1} c_{2(g_1+\theta)} |130\rangle - s_{g_1} c_{g_1} s_{2(g_1+\theta)} |133\rangle \\
&\quad - s_{g_1} c_{g_1} s_{2(g_1+\theta)} |220\rangle - s_{g_1} s_{g_1} c_{2(g_1+\theta)} |223\rangle - c_{g_1} c_{g_1} s_{2(g_1+\theta)} |230\rangle - s_{g_1} c_{g_1} c_{2(g_1+\theta)} |233\rangle, \quad (97)
\end{aligned}$$

between sites 1 and sites 2,3. We further notice we can factor the state on site 2 as $s_{g_1}|2\rangle + c_{g_1}|3\rangle$, leaving a reduced state on sites 1 and 3

$$|\psi'\rangle = c_{g_1} c_{2(g_1+\theta)} |10\rangle - s_{g_1} s_{2(g_1+\theta)} |13\rangle - c_{g_1} s_{2(g_1+\theta)} |20\rangle - s_{g_1} c_{2(g_1+\theta)} |23\rangle. \quad (98)$$

Forming the reduced density matrix on site 1 we get

$$\rho_{\psi'} = (c_{g_1}^2 c_{2(g_1+\theta)}^2 + s_{g_1}^2 s_{2(g_1+\theta)}^2) |1\rangle\langle 1| + (c_{g_1}^2 s_{2(g_1+\theta)}^2 + s_{g_1}^2 c_{2(g_1+\theta)}^2) |2\rangle\langle 2| + (-c_{g_1}^2 + s_{g_1}^2) s_{2(g_1+\theta)} c_{2(g_1+\theta)} (|1\rangle\langle 2| + |2\rangle\langle 1|). \quad (99)$$

Plotting the entanglement entropy of this state (in log base 4) for various g_1 and θ yields Fig. 3(a) of the main text, reproduced here in Fig. 2. We see that the stabilizer has non-trivial operator entanglement for any $g_1 \neq m\pi/2$, $m \in \mathbb{Z}$, so dynamics at these points is surely not Clifford, even in some ‘secretly locally-rotated’ basis.

Lastly, at $t = 3$, there ceases to be any more stabilizers and the state has thermalized to infinite-temperature: $\rho_A(t) = I_A/2^{N_A}$.

-
- [1] Bruno Bertini, Pavel Kos, and Tomaž Prosen. Localized dynamics in the floquet quantum east model. *Phys. Rev. Lett.*, 132:080401, Feb 2024.
 - [2] Bruno Bertini, Cecilia De Fazio, Juan P. Garrahan, and Katja Klobas. Exact quench dynamics of the floquet quantum east model at the deterministic point. *Phys. Rev. Lett.*, 132:120402, Mar 2024.
 - [3] Alessio Lerose, Michael Sonner, and Dmitry A. Abanin. Influence matrix approach to many-body floquet dynamics. *Phys. Rev. X*, 11:021040, May 2021.
 - [4] Michael A. Nielsen and Isaac L. Chuang. *Quantum Computation and Quantum Information*. Cambridge University Press, Cambridge, 2000.